Master‘s Thesis: Mathematical Modeling of a Sea Urchin Gene Regulatory Network

Clemens Kühn

20.12.2006

Abstract

The recent sequencing of the genome of the sea urchin *Strongylocentrotus purpuratus* opens up exciting perspectives for scientists. One of the most exciting and also most challenging goals is to fully understand the mechanisms driving the development of a fertilized egg to an adult organism.

This understanding is achieved by combining experimental and computational methods to establish and validate hypotheses about the developmental process.

In this work, I describe the design of mathematical models of the Sea Urchin gene regulatory network that controls endoderm and mesoderm formation, a key step in embryonic development. The models are loosely based on a network proposed by Davidson et al. and the associated data. They are validated by comparison to various data.

Validation of the constructed models clearly shows that the models suffer from a lack of data. Especially the model based on the proposed network is unable to reproduce the experimental data.

The validation of the models employs a novel approach using sampled parameters to infer features of large ODE models with unknown kinetic parameters.

The present thesis was prepared in the
Evolution and Development Group,
Department Vertebrate Genomics,
Max-Plank Institute for Molecular Genetics

Supervisors:

Prof. Dr. Hans Lehrach
Department Vertebrate Genomics
Max-Plank Institute for Molecular Genetics, Berlin

Dr. Edda Klipp
Departmet Vertebrate Genomic
Computational Systems Biology Group
Max-Plank Institute for Molecular Genetics, Berlin

Acknowledgements

I would like to thank Prof. Dr. Hans Lehrach for enabling me to write this thesis at the Max-Planck-Institute for Molecular Genetics and examination of the thesis. I would also like to thank Dr. Edda Klipp for examination of my thesis and enduring support.

I feel especially indebted to Dr. Albert J. Poustka and Dr. Georgia Panopoulou for their help and guidance.

I am much obliged to Dr. Christoph Wierling for all the help and ideas I received from him.

Furthermore, I must thank Vesna Weise, Maryam Khorasani, Alexander Kühn, Dr. Detlef Groth, Dr. Andrew Hufton and Serguei Baranov for their collegiality and interesting discussions.

I appreciate all my co-students help, distraction and friendship during my course of studies and am especially thankful to Judith Wodke and Anne-Katrin Emde who helped me revise the manuscript.

I am deeply grateful that I can always count on my parents Doris and Gero and my Sister Franziska, who always provided me with vital encouragement and every support I could need.

Katja secured diversion as well as regeneration, enriching my life every day.

List of Abbreviations

Genes/Proteins:

APC *SpAPC*, a hypothesized APC homologue, part of the canonical Wnt-pathway

Axin The (hypothesized) *SpAxin* homologue of *LvAxin* described in [81]

β-catenin *Spβ-catenin*. *Lvβ-catenin* is described in [59]

Blimp1 *SpBlimp1* as described in [54]

Bra *SpBrachyury*,

Brn *SpBrn1/2/4* as described in [86]

Dishevelled The (hypothesized) *SpDishevelled* homologue of *LvDsh* described in [81]

Dkk *SpDickkopf*

Eve *SpEve*

FoxA *SpFoxA* as described in [65]

Frizzled *SpFrizzled*, a hypothesized frizzled homologue that is part of the canonical Wnt-pathway

GataE *SpGataE* as described in [51]

Groucho The (hypothesized) *S.pur.* homologue of *LvGroucho* described in [68]

GSK3β The (hypothesized) *SpGSK3β* homologue of *LvGSK3β* described in [81]

Hox *SpHox11/13b* as described in [37]

Pmar1 *SpPmar1* as described in [64]

Otx *SpOtxβ1/2* as described in [52]

TCF *SpTCF/Lef* as described in [39]

Wnt *SpWnt8* as described in [82]

Methods:

KO Knock-out

MASO Morpholino-substituted antisense oligo nucleotide

QPCR Quantitative real-time ploymerase chain reaction

WMISH Whole mount in situ hybridization

Cell Types:

PMC Primary mesenchyme cells

veg1 Vegetal Layer 1

veg2 Vegetal Layer 2

Miscellaneous:

CV coefficient of variance

GRN Gene regulatory network

hpf Hours post fertilization

M-C Monte-Carlo Methods

mRNA messenger RNA

ODE Ordinary differential equations

SBML Systems Biology Markup Language

S.pur. The sea urchin Strongylocentrotus purpuratus

TF Transcription Factor

List of Figures

Contents

1 Introduction

The sea urchin *Strongylocentrotus purpuratus* (*S.pur.*) is a model organism for development [21]. With the recent finishing of the sequencing of the genome of *S.pur.* [74], a large amount of new data has become available. Using computational techniques to guide experimental research, knowledge of the mechanisms controlling and regulating development of the sea urchin will expand rapidly. One of the most compelling tasks here is to design a mathematical model representing our knowledge of these mechanisms. Using such a model, theories and assumptions concerning developmental mechanisms can be verified or falsified and revised accordingly.

To develop from a fertilized egg into an adult organism, the cells of the developing organism are bound to cleave and differentiate in a determined way. This determined way of cleavage and differentiation is carried out by a complex program of gene expression and cell-cell signaling that must be encoded in the fertilized egg already, i.e. its genome. Maternal transcription factors (TFs) drive the transcription of their target genes in the embryo which cause downstream parts of the developmental program to be activated [20]. The establishment of gradients of secreted molecules along different axes of the growing embryo or among neighboring cells leads to the specification of certain cell types, i.e. the activation of different developmental subprograms [22].

Developmental changes, thus, not only occur inside single cells but also between cells and within groups of cells. Among these macrocellular changes are morphological events, such as gastrulation [19].

Constructing a mathematical model containing all mechanisms that partake in the development from fertilized egg to at least a larval stage is a more than challenging task today. The data needed to construct such a model is still out of reach while the computational methods to tackle a model of such a - necessarily - gigantic, multi-cellular growing system are also unavailable.

A full model of the embryonic development capable of reproducing the major developmental events needs to be comprised of multiple cells, enabling the establishment of gradients as well as morphological changes to occur. An understanding of the processes in the single cell - which ultimately guide the large-scale processes - is inevitable before a full model can be constructed.

Using a model comprised of only one cell to study the small-scale mechanisms controlling development poses other problems. Morphological changes and their effects on molecule gradients or neighboring cells can hardly be taken into account. Molecule gradients must be artificially constructed and adapted to fit the cell type and developmental stage studied. Nevertheless, using a single cell system to model regulatory processes will provide knowledge necessary to construct larger models.

The need to study these small components of the developmental program using the knowledge we have is best illustrated by a metaphor. If one is to interpret the research on single molecules and interactions of single molecules as taking a car apart and analyzing the single screws and bolts, systems biology is the attempt to reassemble the car using the knowledge of the single components. In this sense, I would like to interpret the modeling of single-cell systems as (theoretical) studies on the sparkplugs or cylinders in isolation before reassembling the entire engine. While a sparkplug or a cylinder cannot work in its intended way in isolation, assembling an engine without at least approximate knowledge

of the interplay of the parts and groups of parts will most certainly not result in a working engine.

An elaborate attempt to reconstruct the developmental program from known data is the 'Sea Urchin Endomesoderm Network Model' by Davidson et al [20]. This network graphically displays the presumed links between genes and their respective TFs in three different cell types. It also displays a few interactions between cells. This network only displays the topology of the mathematical model needed to infer the validity of the underlying assumptions.

In this work, I attempt to infer the validity of this network by transferring it into a mathematical model of one cell, modeling different cell types by changes in artificial inputs. These differences are used instead of molecule gradients or other yet unknown components of the full system and will serve the emergence of three different expression patterns from one model without changing either the character or strength of any interaction.

By comparison of *in-silico* and *in-vivo* experiments, the validity of the network is estimated and new experimental approaches can be proposed.

The experimental data underlying this network is rather sparse. For large parts of the model, temporal or spatial expression patterns are not published and TF-gene interactions have only been validated for a few genes [20]. This lack of experimental data restricts the validity of the network itself as well as the validity of the mathematical model.

To construct a mathematical model of high validity, I designed a second model loosely based on the proposed network scheme. This model includes only a small set of well-characterized genes from the above network and data that has not yet been incorporated in the 'Endomesoderm Network'.

The advantage of this small model is not only its manageable size but also the choice of genes: most of them are vital to the development of the sea urchin [22]. The manageable size allows a faster refinement and correction of the model, while the choice of genes implies a fundamental relevancy of the findings from this small model.

As mentioned, the experimental data underlying the network - and thus the derived models - is very sparse. Therefore, nearly all parameters required for the constructed models had to be guessed or estimated. I present one approach for estimating the parameters of the small model and another approach for the analysis of the large model using sampled parameters.

This work aims at amplifying our knowledge and understanding of the development of the sea urchin by critical evaluation of the assumptions made so far. Understanding the development of *S.pur.* is not a trivial goal. As echinoderm, it belongs to the deuterostomes and thus shares certain features with the chordates as well. Because embryonic development is one of the most basic but at the same time one of the most vital mechanisms, the understanding of the developmental mechanisms of *S.pur.* must not be seen isolated but as one step to the understanding of chordate development [21].

2 Background

2.1 Sea Urchins and Development

The following part is designated to give a short introduction to the biological backgrounds of this thesis. It is mainly based on reference [33].

2.1.1 The Sea Urchin as Model Organism

Elementary insights in the mechanisms underlying development have been gathered from the study of sea urchins. As early as 1876 the process of fertilization of a sea urchin egg was shown [36]. Further studies on the fundamentals of development include [38, 26, 10].

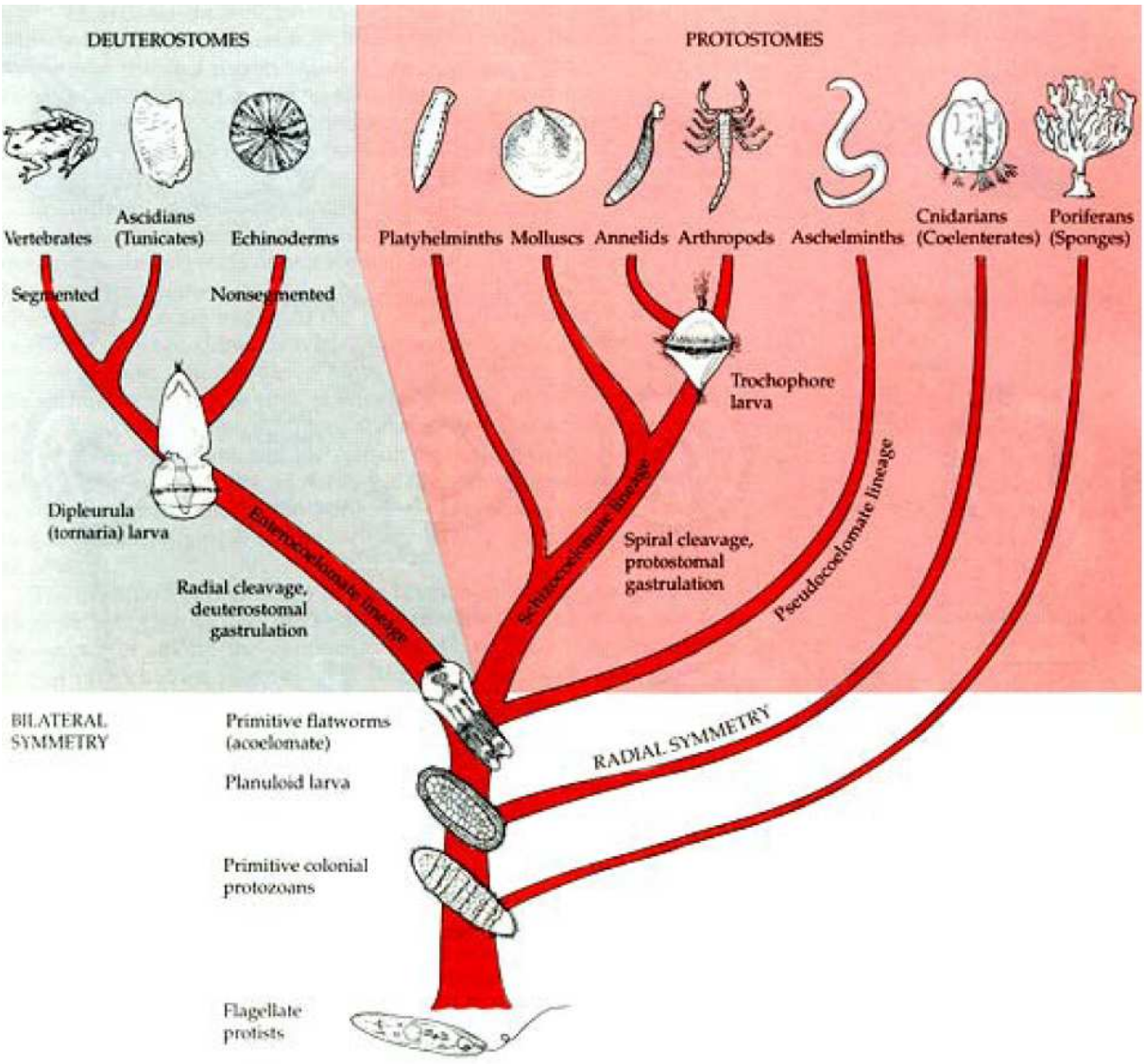

Figure 1: Phylogenetic tree depicting echinoderms and chordates, reproduced from [33]

The choice of the sea urchin as a model system for embryonic development is not

exclusively based on historical reasons. Another reason is the phylogenetic relationship between sea urchins and humans, as outlined in Fig.1. As an echinoderm, the sea urchin belongs to the deuterostomes, as do the chordates. The evolutionary distance between chordates and sea urchins is therefore less than that between chordates and most other model organisms like worms or flies. Although chordates are far more complex than echinoderms, both groups of species share certain features and, of utmost interest here, are similar in many aspects of their embryonic development.

Based on these similarities, the study of the development of the echinoderms will shed light on the development of chordates and, ultimatively, humans as well. This includes the definition of a deutorostome and chordate "tool kit", the set of conserved genes and interactions common to these sets of species [22].

Apart from the reasons mentioned above, there are practical advantages in using the sea urchin for experimental research. Sea urchins are available in large numbers and easy to keep in the laboratory. Embryos are easy to handle and ideal for manipulation and staining. The manipulation of sea urchin embryos is possible in a variety of ways [27] and gene transfer into the eggs is especially simple [21].

2.1.2 Embryogenesis of the Sea Urchin

The sea urchin develops from the fertilized egg into an embryo that further develops into a larvae from which the adult animal is formed. In this work, I focus on the embryonic development from the fertilized egg to about 40 hours post fertilization (hpf). During this time, the embryo undergoes a series of morphological changes and the foundations of most of the adult animal's cell types and tissues are defined by the end of this period.

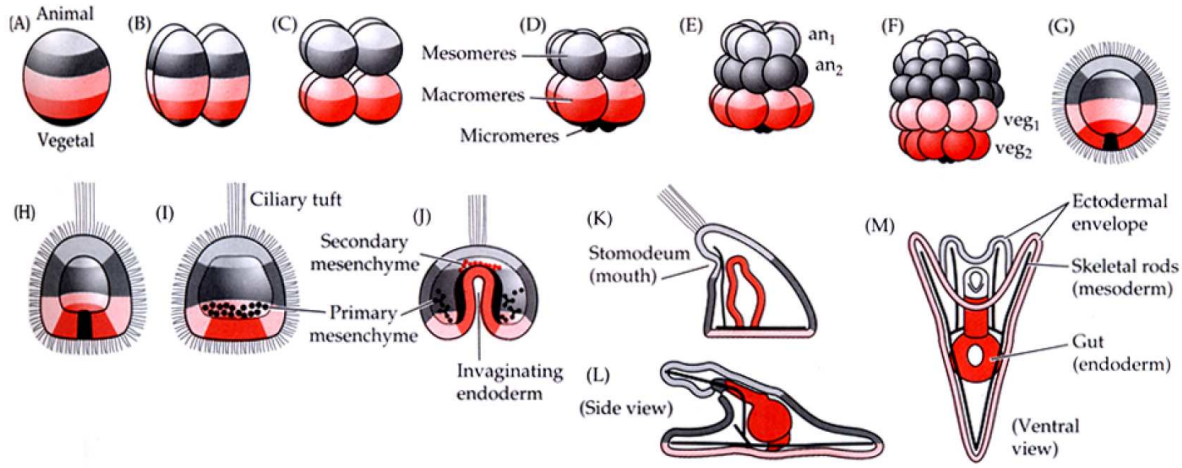

Figure 2: Overview of the embryonic development of the sea urchin, reproduced from [33], from fertilized egg (A), early cleavages (B,C,D,E) to blastula (F/G). Gastrulation movements are shown in (H, I, J) and later development to larvae (K,L,M).

The first two cleavages of the fertilized egg are synchronously as well in regard to cell size as in regard to cleavage intervals among cells. Within the next cleavages, cells of different size are formed, roughly outlining later embryonic territories. A schematic overview of these processes is shown in Fig.2.

Experimental [16, 58] and computational [12] studies suggest that the different size of the resulting cells cause - among other mechanisms - an asynchronization of cleavage intervals.

In the 128 cell blastula stage, which arises about 6.5 *hpf* in *S.pur.*, all future territories of the developing embryo are outlined: oral and aboral ectoderm, the vegetal plate (veg1, veg2), primary mesenchyme cells (PMC) and small micromeres.

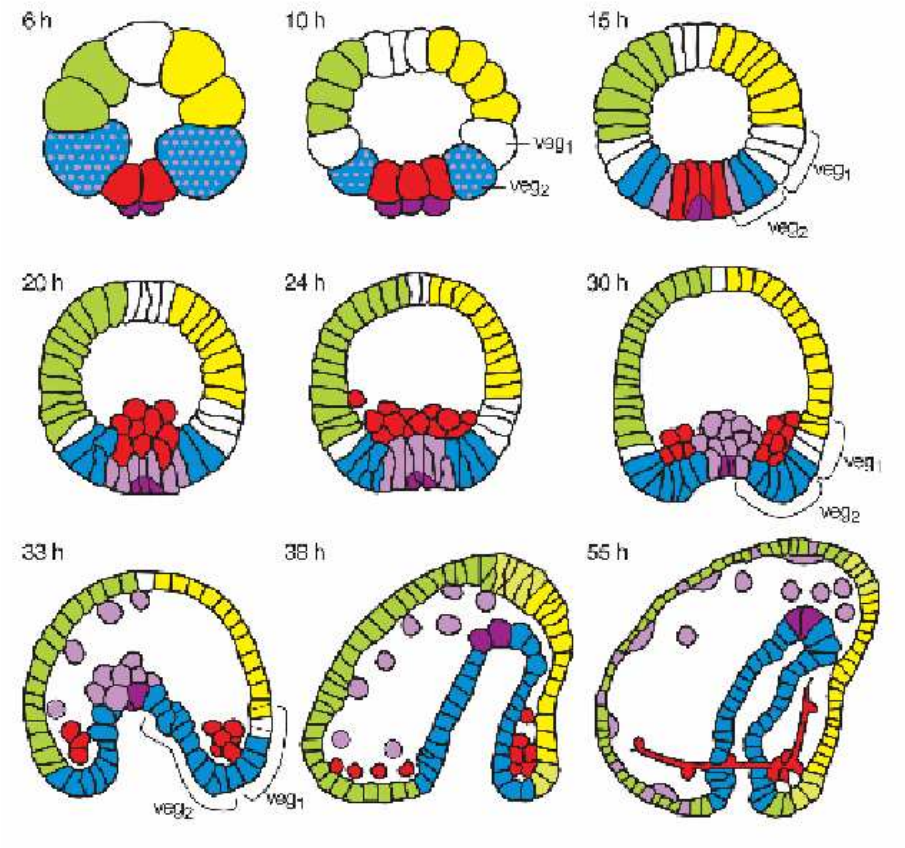

Figure 3: Development of the sea urchin from early to late Gastrula, reproduced from [53]. Dark purple depicts the small micromere precursors of mesoderm, red are PMC cells, light purple is veg2 mesoderm, blue veg2 endoderm and green and yellow depict ectoderm territories. PMC ingression is visible in the second row, archenteron formation 30 to 56 *hpf*.

By the end of the blastula stage, Gastrulation begins with the ingression of the PMC cells. After the PMC cells form a ring along the vegetal side of the embryo, cells from the vegetal plate invaginate to form the archenteron. The archenteron is elongated until it reaches and penetrates the ectodermal side of the embryo. Further morphological changes then form the pluteus larvae. These morphological changes are sketched in Fig.3.

Although the sequence of these events is similar among all indirect developing sea urchins, the exact time at which the events occur varies between species.

The number of cells is grows throughout the developmental phases of the embryo even while morphological changes occur [57].

2.1.3 Developmental Mechanisms

General mechanisms of gene regulation have been identified for various scenarios [66]. General developmental mechanisms of gene regulation might thus also be identified. The identification of those general mechanisms would greatly ease the construction of developmental gene regulatory networks (GRNs).

Among these mechanisms are certainly asymmetric cell divisions that change the nuclear complement of TFs and extracellular gradients among embryonic axes [63]. These mechanisms are easy to observe and then link to developmental functions. For example, if a gene's product is observed to constitute a gradient in the embryo, it is likely to be important for developmental processes and targets of this protein should be analyzed for possible developmental function.

Identifying regulatory mechanisms common to families of networks is done by topological analysis. One approach to classify families of GRNs is to measure transcription cascade lengths of sequential regulation [70]. It has been shown that developmental GRNs generally exhibit a greater cascade length than sensory GRNs (i.e. GRNs that mediate the transcriptional response of a cell to a given outside stimulus) [70]. Furthermore, indications were found that cascade length is directly correlated to response delay by about one cell cycle round of response time per cascade step [70]. This finding is of more general nature and is not necessarily helpful for the design of individual developmental GRNs but might prove powerful when attempting to use one known developmental GRN to establish another, unknown developmental GRN. Another approach to characterize networks based on topological features is given in section 2.2.1.

A very specific and yet general study was performed, comparing and analyzing the design of known signaling pathways regulating development [6]. In this study, it has been shown that these developmental signaling pathways commonly exhibit three mechanisms: activator insufficiency, cooperative activation and default repression. The results are summarized in Fig.4.

Activator insufficiency describes the fact that signaling activity alone is often insufficient to activate target genes. Activation of target genes can only occur when a locally present activatory TF binds to the target gene's regulatory unit in addition to the signaling activity mediating TF (cooperative activation). To minimize ectopic expression caused by local activators in absence of signaling activity, default repression is employed. This default repression is often mediated by the same TF as the positive signaling activity. For an example of those habits, see the Wnt-pathway in section 4.1.1.

2.1.4 Experimental Methods

Studying the development of the sea urchin, diverse experimental techniques have been applied to this model organism. In the following section, I give a short introduction to the experimental methods that were used to obtain the data underlying the modeling of sea urchin development.

Information inevitable to the design of regulatory networks are temporal expression profiles, i.e. measuring transcript numbers for a given gene at different time points. To measure transcript numbers, mRNA is isolated from an organism at the timepoints for which transcription numbers are to be determined. These samples are amplified via QPCR (quantitative real-time PCR) until a certain threshold is reached. By comparison to se-

quences for which transcript number is known (usually *Ubiquitin*), the transcript number in question is determined. For details of the method, see [37].

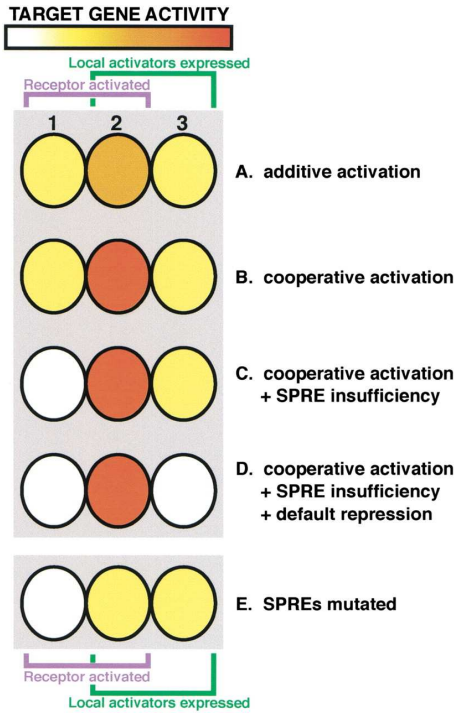

Figure 4: Common habits of developmental signaling pathways, reproduced from [6]

To this date, transcript numbers of genes in the sea urchin embryo are measured per embryo. Thus the number of transcripts in all territories is measured. Additionally, transcript numbers are not directly linked to activation or inactivation of transcription since transcript numbers are also regulated via their stability as reviewed in [23].

Besides the temporal expression, knowledge of the spatiotemporal expression pattern (or where a gene is expressed at what time) is of elementary importance to the study of regulatory systems. To detect spatial expression, embryos are stained using whole mount in situ hybridization (WMISH) as outlined in [62]. WMISH produces a staining that is specific to a certain sequence and thus allows to infer the territory of expression of a certain gene at the developmental time point at which the embryo was fixed. In contrast to the method described above, WMISH can only generate qualitative expression data.

To infer regulatory linkages between TFs, a widely used practise is to perturb the expression of one TF and compare the transcript numbers of genes likely to be effected under this perturbation with transcript numbers determined in unperturbed embryos.

The perturbation can be of various kinds: A gene can be knocked out or the translation of a gene is repressed by injection of antisense morpholino oligonucleotides to reduce the effect of the perturbed gene. The effect of a TF on its target genes is forced negative by fusion with the Engrailed repressor domain. The amount of available mRNA of a given gene can be increased by injection of extra mRNA to cause ectopic expression. For details on these methods and their application to the sea urchin, see [27].

As described above, quantitative temporal expression data is determined for the entire embryo. The qualitative spatiotemporal expression data specifies the territory of the embryo in which a gene is expressed at a given timepoint. By combining this information, one can infer the quantitative temporal expression profile of a certain gene in the cells of a given territory. The only additional knowledge needed is the number of cells comprising the embryonic territories of interest at the measured time points.

For the early embryo, this data is available in the form of fate maps and cell counts. These are based on studies of the cell cycle and unequal cleavage events in the early sea urchin embryo [19, 77, 58, 16]. Later studies employ stereo imaging and 3d-reconstruction to infer cell numbers for later stages of development [75, 57].

2.2 Mathematical Modeling of Gene Regulatory Networks

Mathematical models allow for the formalization of hypotheses about a system and to validate these hypotheses. Using an appropriate formalism, nearly all systems imagineable can be modelled. Using computational tools, the behavior of such a model is tangible to simulation and analysis.

In molecular biology, models are used to validate hypotheses arising from experimental data. The model represents the current understanding of the studied system and by comparison between simulation and experimental results, the model is revised until it satisfactory reproduces the experimental data, as outlined in Fig.5 [43].

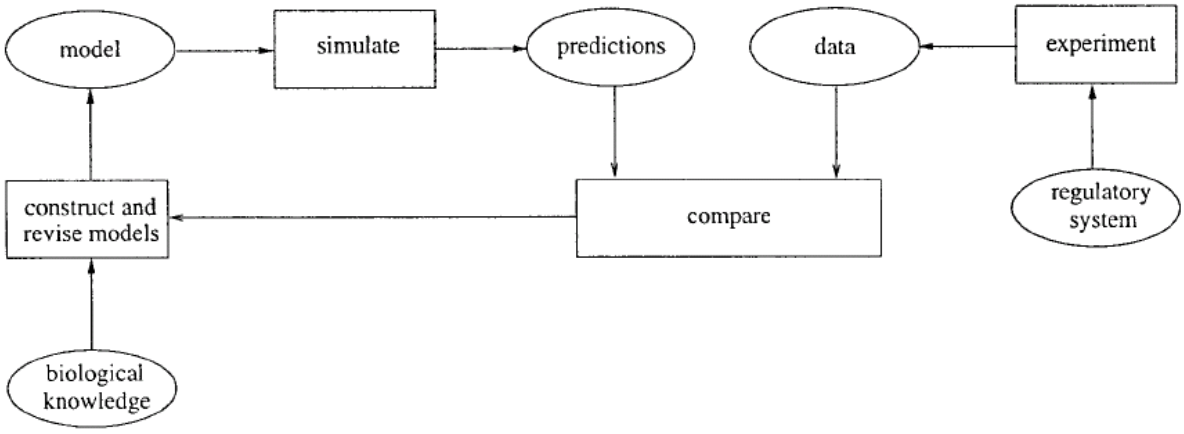

Figure 5: Analysis of biological models, according to [43]

Besides simulating the behavior of the model, the model can be analyzed to determine structural and dynamic properties. The methods applicable for simulation and analysis of a model depend on the choice of the modeling formalism. The review by Hidde de Jong [43] gives a very good overview of the different methods. Here, I will give a short introduction to the methods used in this work.

2.2.1 Directed Graphs

A directed graph G consists of a set of nodes V and a set of edges E, where an edge e is a tuple i, j, with $i, j \in V$ where i denotes the source and j denotes the target of e.

The analysis of topological features of a system is one application to directed graphs. Determining the connectivity distribution of a graph enables a classification of the network. Families of networks with a similar connectivity distribution exhibit similar properties.

Most biological networks belong to the so called scale-free networks. Characteristic of scale-free networks is the existence of a large number of edges with a low connectivity contrasted by the existence of a few highly connected nodes resulting in a typical connectivity distribution. The probability $P(k)$ of a node having k incoming or outgoing edges is roughly proportional to $k^{-\gamma}$. A scale free topology gives rise to a high robustness against random deletion of nodes at the cost of a low robustness against directed deletion

of the highly connected nodes [5]. As most biological mechanisms rely on a high stability against random perturbations (arising, for example, from random mutations), the scale free network is the expected type of network of a GRN.

Extracting and analyzing network motifs is another powerful tool to characterize a directed graph. Network motifs are significant patterns of connection, as exemplified in Fig.6.

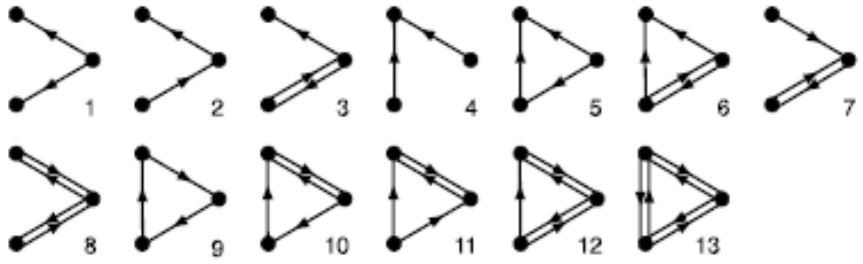

Figure 6: All possible three-node Network Motifs of directed graphs, reproduced from [60]

Certain network motifs can be linked to certain functions, i.e. the feed forward loop is a common motif in regulatory sysems. Networks can be characterized by comparing the accumulation of different network motifs in one graph to the expected accumulation of these motifs in a random graph of comparable size and connectivity. This comparison often employs z-scores. Using the z-scores of different motifs, it has been shown that certain networks exhibit characteristic patterns of z-scores [60].

Given a directed graph, the program mfinder [44] detects network motifs and calculates z-scores.

Further studies in this field might reveal why certain types of networks exhibit distinct patterns of network motif accumulation as well as dynamic properties of certain motif assemblies.

2.2.2 Boolean Models

A Boolean model consists of a set X of Boolean variables and a set of Boolean functions B. The state of a variable $x_i \in X$ at time point $t + 1$ is determined by evaluating the corresponding function $b_i(t)$. The state S of a Boolean model at time point t is the vector consisting of $x_i(t)$ for all x_i in X [43]. An example of a simple Boolean model is given in Fig.7.

To construct a Boolean model of a GRN, the genes are expressed as Boolean variables and the interactions between genes are expressed in terms of Boolean functions. This approach assumes that a gene has exactly two states of activity. It must either be active or inactive, a strong simplification of reality [43].

In spite of this simplification, it is possible to identify steady states or oscillations from Boolean models and perform basic simulations of the system on them [43]. Boolean models have the advantage of requiring only very basic knowledge of the system compared to other modeling approaches. They are therefore useful as schemes for more detailed

models, with which the basic topology and nature of interactions in the model can be tested.

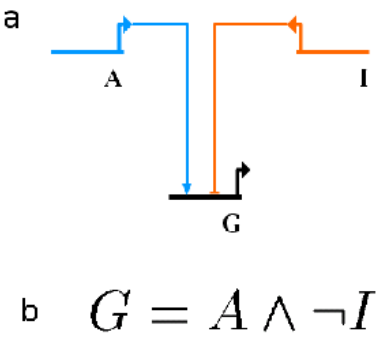

c

A	I	G
0	0	0
0	1	0
1	0	1
1	1	0

b $G = A \wedge \neg I$

Figure 7: Example of a Boolean model of a GRN consisting of a gene coding for an activatory TF A, a gene coding for an inhibitory TF I and an effected gene G. Shown are the topology of the network (a), the Boolean formula controlling the state of G (b) and a truth table with the state of G relative to the states of its inputs A and I. The graphic representation of the network topology was constructed using BioTapestry software. [56]

Extensions and variations of Boolean models, such as generalized logical models, have many distinguished applications and allow for a wide range of analysis, such as model checking [43].

2.2.3 Ordinary Differential Equation Models

In ordinary differential equation (ODE) models, the concentrations of the substances are modeled as time-dependent variables from the realm of the positive real numbers. A variable's concentration x at time t is determined by an initial concentration and a differential equation of the form $\frac{dx_i}{dt} = f(x_1, x_2, ...x_n, p_1, p_2, ...p_n, t)$, where $x_1, x_2, ...x_n$ is the set of all variables and $p_1, p_2, ...p_n$ is the set of all parameters [43]. $f(\mathbf{x})$ usually consists of one or more synthesis terms and one or more degradation terms. These synthesis and degradation terms are generally rate laws that determine the speed of the modeled reaction. An example of a simple ODE model is given in Fig.8.

Once a vector of initial concentrations is chosen and all necessary parameters are identified, it is possible to compute a numerical simulation. Computational tools for the design and numerical simulation of ODE models, such as CellDesigner [31], are widely available. Due to this availability and the wide range of model analysis applicable to ODE models, this is a very popular modeling formalism, although most properties of models are determinable using simpler modeling formalisms.

In general, not all parameters are available from literature. Thus, parameters are often chosen in a way that enables the model to reproduce the given experimental data. Depending on the available data, parameters can be estimated using computational tools like SBML-PET [87].

Once the parameter values are obtained, it is possible to simulate and analyze an ODE model. Stable states of the system can be determined and their stability is accessible [43]. Metabolic control theory contains a set of tools to analyze the sensitivity of steady states to parameter or concentration changes [45].

2.2.4 Parameter Estimation

With the emergence of systems biology, parameter estimation is growing in importance as well: For an ODE model, a great number of parameters is required. These parameters are - theoretically - obtained from experimental biology. In practice, modeling of biological processes aims at improving the understanding of these processes. Therefore,

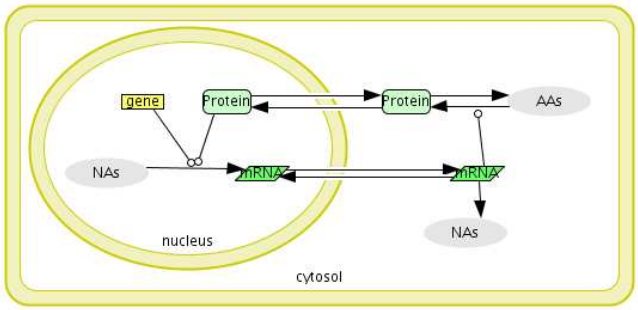

rate laws:

$v_{transcription} = k_{transcription} \cdot [Gene] \cdot \frac{[Protein_{nucleus}]}{c_{transcription} \cdot [Protein_{nucleus}]} \cdot [NAs_{nuclear}]$

$v_{mRNA_degradation} = k_{mRNA_degradation} \cdot [mRNA_{cytosol}]$

$v_{mRNA_export} = k_{mRNA_transport} \cdot [mRNA_{cytosol}]$

$v_{mRNA_import} = k_{mRNA_transport} \cdot [mRNA_{nucleus}]$

$v_{translation} = k_{translation} \cdot [mRNA_{cytosol}] \cdot [AAs]$

$v_{Protein_degradation} = k_{Protein_degradation} \cdot [Protein_{cytosol}]$

$v_{Protein_export} = k_{Protein_transport} \cdot [Protein_{cytosol}]$

$v_{Protein_import} = k_{Protein_transport} \cdot [Protein_{nucleus}]$

differential equations:

$\frac{d[Gene]}{dt} = 0$

$\frac{d[AAs]}{dt} = 0$

$\frac{d[NAs]}{dt} = 0$

$\frac{d[mRNA_{nucleus}]}{dt} = v_{transcription} - v_{mRNA_export} + v_{mRNA_import}$

$\frac{d[mRNA_{cytosol}]}{dt} = v_{mRNA_export} - v_{mRNA_import} - v_{mRNA_degradation}$

$\frac{d[Protein_{nucleus}]}{dt} = v_{translation} - v_{Protein_import} + v_{Protein_export} - v_{Protein_degradation}$

$\frac{d[Protein_{cytosol}]}{dt} = v_{Protein_import} + v_{Protein_export}$

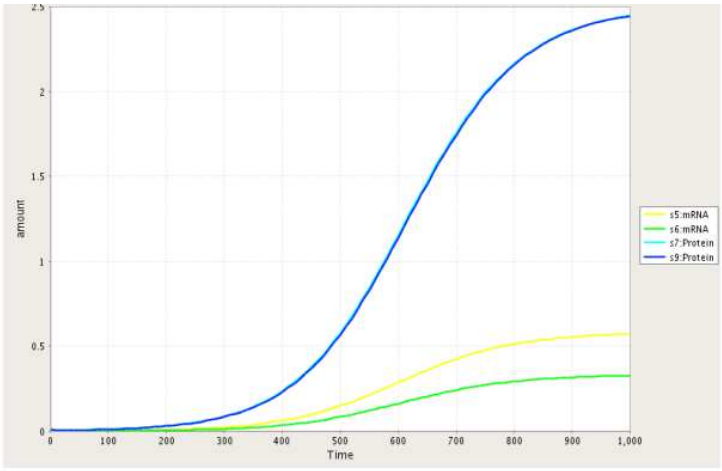

initial and parameter values

$Gene = AAs = NAs = 1$

$mRNA_{nucleus} = mRNA_{cytosol} = Protein_{cytosol}$

$Protein_{nucleus} = 0.01$

$k_{Transport} = 0.4$

$k_{transcription} = 0.5$

$k_{translation} = 1.5$

$k_{mRNA_degradation} = 0.3$

$k_{Protein_degradation} = 0.2$

Figure 8: Graphical representation of an ODE model containing different compartments. Arrows in the topology represent reactions. Arrows crossing boundaries indicate transport reactions. Lines with circles represent catalysis. NAs and AAs are the pools of single nucleic and amino acids. The network contains a positive feedback loop. Notice that just a little initial amount of the TF results in a stable steady state with high protein and mRNA concentration. The model was designed and simulated using CellDesigner3.2 [31].

the mechanisms underlying the model are not fully understood. Thus, some parameters are unknown. Some of the parameters necessary are impossible to measure using todays experimental methods. Thus, the need to estimate parameters is growing as the number of models is increasing.

The approach I employ here is to estimate the unknown parameters in such a way that the simulation results resemble a set of experimental data. SBML-PET [87] implements this approach using an evolutionary algorithm based on Stochastic Ranking Evolution Strategy [42].

2.3 Automatic Model Reconstruction from Experimental Data

To construct a mathematical model of a system, the experimental data thereof has to be evaluated and analyzed. When the systems in question exhibit enough similarity and the underlying mechanisms are thoroughly understood, this evaluation and analysis of the experimental data can be automated.

An advantage of this automation would be that the amount of time and labor to construct a mathematical model would be greatly reduced. Another advantage would be that the resulting models could be directly compared and personal bias of a researcher cannot affect the resulting model.

On the other hand, automatically inferring a mathematical model directly from experimental data demands detailed and standardized available data, exact knowledge of all possible underlying mechanisms and a sophisticated algorithm.

Creating an algorithm that can produce a sensible mathematical model even from sparse data of a GRN would thus revolutionize the way mathematical models of GRNs are constructed.

Although much reseach is done on that topic (see, for example [46]) and various approaches have been proposed, the anticipated revolution has not taken place yet due to the complexity of the task.

Altogether, the computational tools available combined with the experimental data can aid in the construction of a mathematical model, for example predict TF-binding sites from sequence data. But the complete task of designing and refining the mathematical model cannot - yet - be fully automated.

2.4 Monte-Carlo Methods

Monte-Carlo methods are based on the law of great numbers: Repeating a calculation that involves a great amount of freedom with a great number of different parameters, the calculation is assumed to approximate the exact behavior that was previously inaccessible [30].

If a model of a biochemical system can be assumed to be relatively robust to parameter changes and parameters are sampled from a reasonably applicable random distribution, key features of the system are expected to be (qualitatively) conserved when enough different parameter sets are used.

These, necessarily robust, features are distinguishable from dynamical features that heavily depend on parameters once the parameter values are obtained.

Estimating parameters is based on the assumption that the correct parameters are a prerequisite for the model to exhibit the expected behavior. Many biological networks exhibit a strong robustness to changes of parameters [18, 4], indicating that the system itself is rather indifferent towards parameter changes within a reasonable range.

These findings imply that the key features of a system are accessible with very limited knowledge of the exact parameters. This idea is exploited in generalized logical networks [43]. I want to employ another approach based on Monte-Carlo methods: A large number of parameter sets is sampled and employed in the simulation of ODE models. Comparing the simulation results of perturbed and unperturbed models enables the assessment of downstream effects of these perturbations. Aligning these results with experimental data might allow for a rough evaluation of the model's validity.

2.5 SBML - Systems Biology Markup Language

SBML is a computer-readable format for the implementation of models of biochemical systems. It is based on XML and uses MathML to encode mathematical formulas. It is widely applicable to most biochemical systems and readable by a multitude of software tools. An advantage as well as a disadvantage of SBML is its wide applicability and neutrality towards software encoding. This allows a wide variety of programs to use SBML while each program can process the model differently. Thus, two SBML-compliant programs need not necessarily produce the same output when performing similar tasks (e.g. simulation of the model) on a model. For detailed information about SBML, see [40, 29, 2].

3 Data

3.1 Network Scheme and Perturbation Data

This thesis is mainly based on the 'Sea Urchin Endomesoderm Network' [20] and associated papers. Other resources are complementary publications on experimental data as well as unpublished results generated within the group of Evolution and Development at the Max-Planck-Institute for Molecular Genetics, Berlin [1]. The most important sources of data are introduced and explained here.

Although introduced as the 'Endomesoderm Network Model', the endomesoderm network is not a distinguished mathematical model (although it certainly is a directed graph) but rather a network of interacting genes. The choice of interactions is based on the interpretation of perturbation data, which will be explained later. The endomesoderm network, as depicted in Fig.9, is a graphical representation of the network. It is enlightening because it presents a visualization of inferred and validated interactions, thus summarizing the experimental data available. It is, at the same time confusing because TFs seem to have different sets of targets depending on the cell type.

Assuming a gene's regulatory unit remains invariable, this difference in targets of a TF is almost impossible. Although it is possible that a TF-gene interaction that is active in one cell type is inactive in another cell type due to specific (competitive) repressors or repression of the TFs transcription or translation. In this case, the possibility of an interaction remains and must be taken into account. The only case in which a TF cannot

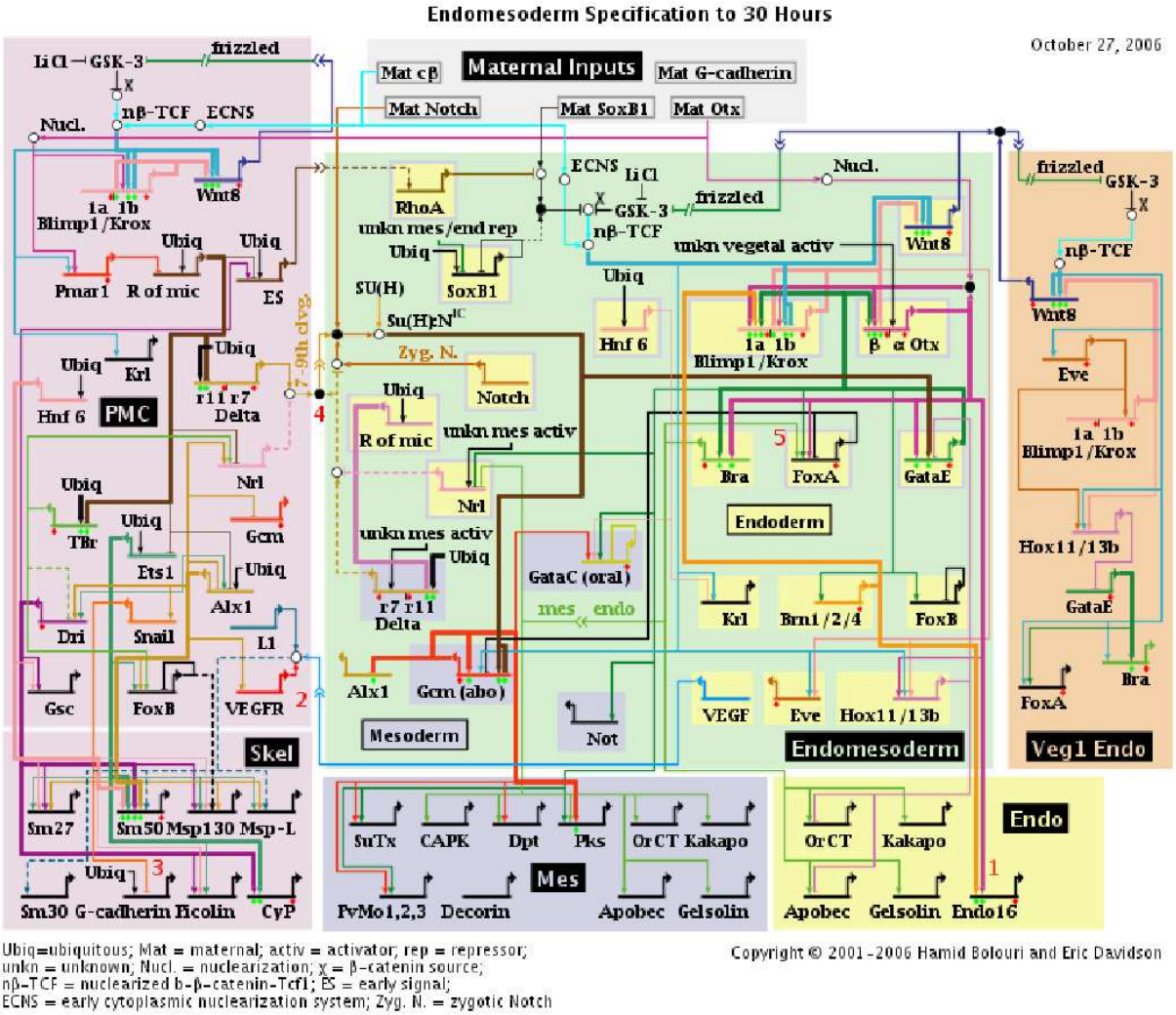

Figure 9: Endomesoderm Network, 27 October 2006, reproduced from [3]. Bars with arrow represent genes, Text insets indicate Proteins or complex pathways (ECNS ≡ early cytoplasmatic nuclearization system) black and white circles indicate protein interactions. Arrows indicate positive inputs to protein interactions and regulatory regions of genes, barred lines likewise indicate inhibitory inputs. Portions of the Network are colored to indicate the spatial domain of transcription in the early embryo.

bind to a previously available binding site on a gene is when the structure of the DNA has been modified via chromatin reorganization. Chromatin reorganization is not outruled as a molecular mechanism of development, but rather improbable [19].

Another possible explanation for these different interactions is that the downstream interactions are a result of indirect effects wrongly interpreted as direct effects. One possible case here is that gene A is perceived as activator for gene C in just one cell type. The real activator of C might in fact be a gene B that is activated, in part, by A. Once the intermediate TFs or spatially restricted competitive inhibitors are determined, these irregularities are expectedly eliminated. This explanation is complementary to the habits outlined in section 2.1.3.

The network is far from complete. As of today, about 62 genes constitute the network. A recent study [37] has revealed 96 homeobox TFs in *S.pur.* Out of these, 65% are expressed within the first 48 hours of development, thus indicating a role in developmental processes for 62 homeobox TFs alone. Because the network does most certainly not consist exclusively of homeobox TFs, this finding illustrates the incompleteness of the network.

This incompleteness is allowed for by regularly updating the network to integrate new experimental data. It is further demonstrated by the vast number of TFs labelled 'Ubiq' in Fig.9. These ubiquitous TFs are basically placeholders either for unidentified interactions or unidentified TFs.

The representation of protein-protein interactions as well as signaling to and from the extracellular space are merely sketched. This lack of detail certainly serves the clarity of the network, but it confines its abilities as a realistic representation.

The network is mainly designed from perturbation and expression data
[20, 3]. The perturbation data, as far as documented [3], results from the three different experimental setups as explained above.

Another prominent source for data was the Evolution and Development Group [1]. Here, experimental research focuses on genes that are not yet included in [3] but are expected to be important regulators of development.

3.2 Expression Data and Fate Maps

Quantitative temporal expression data is available for some genes in the sea urchin GRN for the specification of endomesoderm. As described above, the number of transcripts per embryo of a given gene is measured at different time points.

For the set of genes that is later used to construct the core model, such measurements could be obtained from literature or ongoing work by A. Kühn, Dr. A.J. Poustka and Dr. G. Panopoulou. This set includes *Blimp1* [54], *Bra* (ongoing work), *Brn* [86], *Dkk* ([49] and ongoing work), *FoxA* [65], *GataE* [51], *Hox* [37], *Otx* [52], *Pmar1* [64] and *Wnt8* [82].

Transcript numbers per embryo or generally per organism are not necessarily equal to the transcriptional activation of a gene.

First, one must discriminate between transcript numbers and transcriptional activity. Transcript numbers are dependent on transcriptional activity, but other sources can influence the transcript number as well. If transcriptional activity remains unaltered but the half life of the transcripts is modified, the number of transcripts will rise or fall accordingly.

Second, transcript numbers per embryo are not transcript numbers per cell. This might seem obvious, but the resulting implications have not yet been applied.

The embryo consists of a growing number of cells which belong to different cell types or embryonic territories. The different territories grow at different rates.

A gene is almost never expressed at the same rate throughout the whole embryo. Most regulatory genes' expression is in fact confined to a distinct territory. Some genes might switch their territory of expression or emit complex spatial expression patterns.

Assume now that gene A is expressed in the whole embryo. If the number of transcripts remains constant over a phase of observation and influences on transcript number other than transcriptional activity are ruled out, a seemingly obvious conclusion is that transcriptional activity is declining: As the number of cells is growing and the number of total transcripts remains stable, the number of transcripts per cell is declining.

In general, the number of transcripts per cell can be calculated by dividing the number of transcripts by the number of cells expressing the gene. For genes with simple expression patterns, this seems quite simple: observe the territory where the gene is expressed at a given time point via WMISH and infer the number of cells that constitute this territory at the time point studied. The number of cells that make up different embryonic territories is described in [77, 58, 16, 75, 57]. The number of cells for each cell type inferred at various timepoints is depicted in Fig.10. The results presented are rough estimates based on experimental results from different species (*Lytechinus variegatus* apart from *S.pur.*) and different methods.

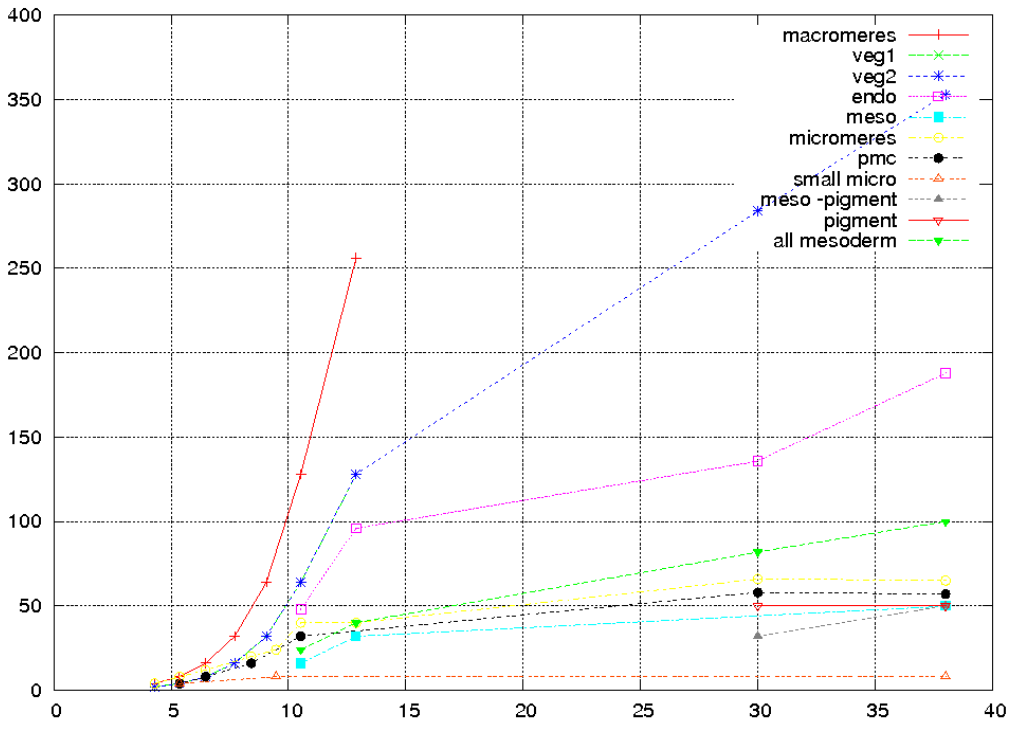

Figure 10: Inferred number of cells for each cell type as described in the text. The x-axis depicts hpf, the y-axis shows numbers of cells. Numbers of cells were inferred at the marked timepoints only. For references to the original data, see section 3.2.

This simple approach can - in most cases - only serve as a basic guideline, since

gradients in transcriptional activity among cells (as arise from gradients of extracellular signalling molecules) cannot be inferred this way. This approach is also insufficient to account for more complex spatial expression patterns, where, for example, gene A is expressed in a certain territory T and after a certain while A's expression switches to territory U. If the expression in territory T and U is temporally overlapping, the transcriptional activity of gene A in cells of either T or U is indiscriminable from the other. In Fig.11, the expression of *FoxA* exhibits an oscillating pattern. Whether this pattern arises from transcriptional regulation in each cell or from changes in the number of cells expressing the gene is unknown.

In general, I expect this approach to produce significantly more valid data, although it surely lacks refinement. The results of according recalculations for some genes of the core model are exemplified in Fig.11

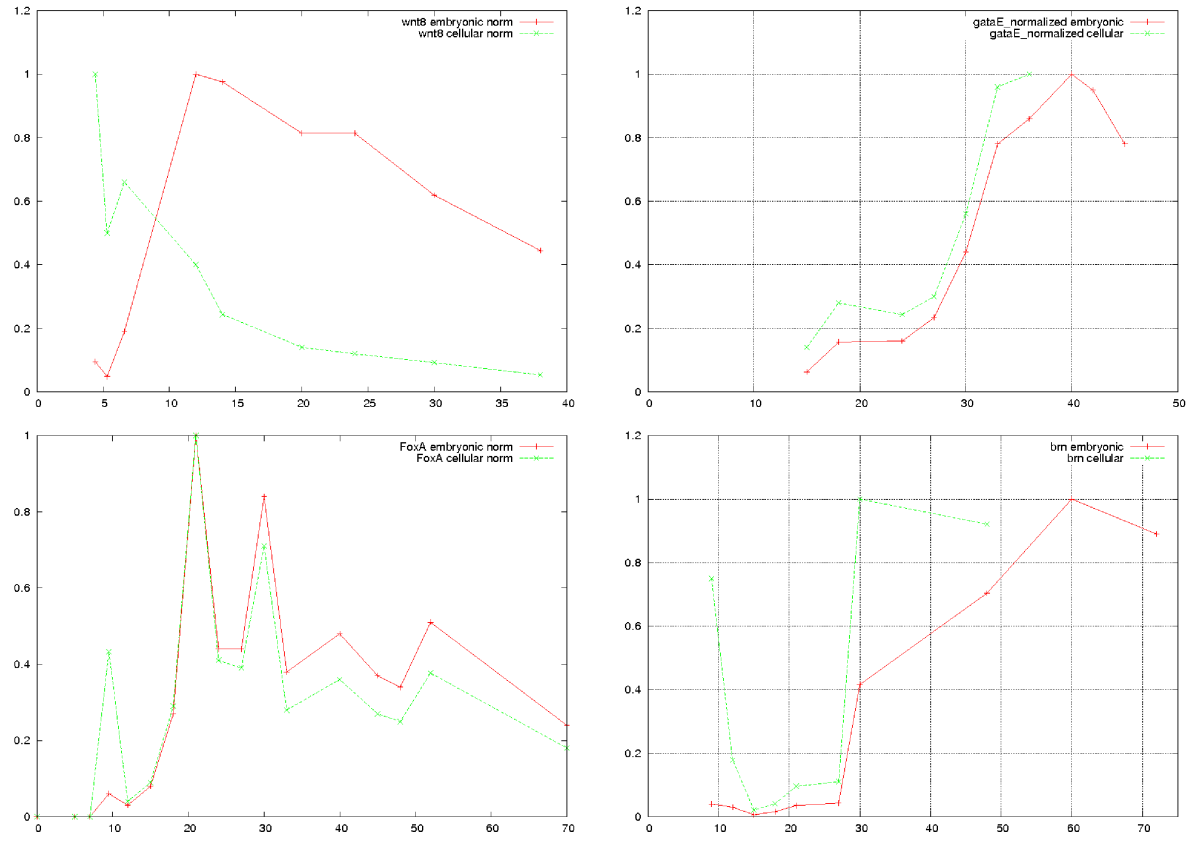

Figure 11: Expression of several genes of the endomesoderm Network. X-axis shows hpf, y-axis shows relative expression levels. Each panel shows the relative expression per embryo (as obtained from literature) and per cell expressing the gene (recalculated from the original data). For details of the data and the recalculations, see 3.2. The expression level is normalized to the respective maximum for each curve. The absolute maxima of cellular and embryonic expression usually differ by several orders of magnitude.

4 Modeling

4.1 Summary of Assumptions and Approaches

The complex network controlling the development of an organism comprises a large set of different interactions with the interactions between TFs and their target genes in each cell that lead to distinct patterns of gene expression at its heart.

This microscopic set of interactions is as well the source for macroscopic interactions like the constitution of extracellular gradients as their target. While the microscopic interactions constitute the macroscopic events, macroscopic events and interactions play a crucial role in regulating the microscopic interactions.

To construct a simple model catching both the macroscopic and the microscopic interactions is a task far too complex to tackle in this thesis. Here, I attempt to construct a mathematical model of the microscopic interactions at the heart of this complex system.

As this attempt focuses on intracellular processes, the model will consist of only one cell. Interactions with the surrounding medium are modelled as artificial inputs that do not emerge from the model but are controlled by external input.

The basis of this model is the proposed 'Endomesoderm Network' as described in [20], an updated version available on [3]. This network is proposed as the GRN controlling specification of the endoderm, mesoderm and PMC cell lines. The mathematical model therefore must enable the reproduction of three different sets of temporal expression patterns based on the different external inputs. The proposed model consists of about 76 species and about 190 interactions in its actual form. These species are not exclusively genes but also consist of proteins, signaling cascades and protein complexes. Most of these non-gene species are only sketched since the underlying mechanisms are partly as complex as the entire network itself (see work on Delta-Notch and Wnt singlaing pathways).

4.1.1 The Canonical Wnt-Pathway

A direct example of the lack of protein-interaction representation in the 'Endomesoderm Network' is the canonical Wnt-pathway and its role in the endomesoderm network: It has been shown that nuclear β-catenin is necessary for the specification of vegetal cell fates in the sea urchin [55]. Further studies have revealed that Frizzled [14], GSK3β [28], Dishevelled [81] and TCF [78] are involved in this process. All of these are involved in the canonical Wnt-pathway. Competitive binding of Groucho and β-catenin to TCF in the sea urchin has also been experimentally shown. TCF can act as transcriptional inhibitor (when Groucho is bound) or transcriptional activator (when β-catenin is bound) [68, 17]. As this data suggests, the canonical Wnt-pathway is assumed to be conserved in *S.pur.* [15].

The canonical Wnt-pathway plays a crucial role in the early specification events of *S.pur.*. Extracellular Wnt binds to the Frizzled receptor which in turn activates Dishevelled. Activated Dishevelled inhibits the degradation of β-catenin via the GSK3β/Axin/APC complex. This degradation is the main regulatory step in the regulation of nuclear β-catenin concentration and thus the role of TCF, although several other interactions can positively or negatively effect this pathway, which is only briefly sketched in the network diagram in Fig.9. As illustrated by Fig.12, Wnt thereby controls the transcriptional effect of TCF which, as depicted in Fig.9 again influences Wnt. This feedback leads to a strong

influence of the exact gradient of β-catenin/TCF and Groucho/TCF and a bistability of the resulting network: If *Wnt* is expressed, β-catenin accumulates and can thus bind to TCF to maintain Wnt expression. If Wnt is absent, β-catenin is degraded and TCF is mainly bound to Groucho, which leads to an even stronger downregulation of Wnt expression.

The core components of this evolutionary well conserved pathway have been modeled and analyzed in [48, 50]. An overview of the topology of these models is given in Fig.12. This network's function is an example of the common habits of developmental signaling pathways as described in section 2.1.3.

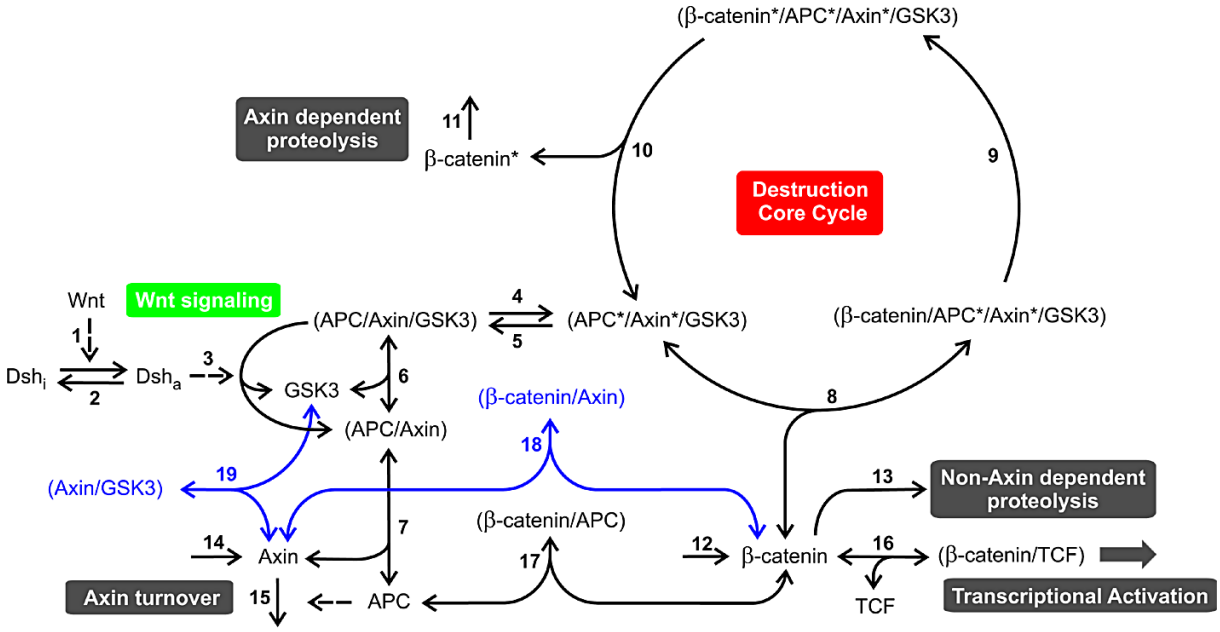

Figure 12: Schematic diagram of the Wnt-pathway, reproduced from [50]

This well documented pathway is an example of where I was able to improve the proposed network by integrating new data. Other pathways, for example the delta-notch pathway are not as well documented in the sea urchin and could therefore not yet be integrated.

4.1.2 Modeling of Artificial Inputs

Since the models are incomplete and consist of only one cell which is influenced by its environment, certain components are missing. Regardless of the origin of these missing components, their influence must be integrated into the model.

Most of the artificial input's activity has been qualitatively characterized [3]. Integration of artificial inputs into Boolean models is therefore obvious and straightforward.

To integrate the inputs into ODE models and conserve steadiness of the system, a more sophisticated approach is necessary.

All programs used here for the simulation of ODE models (CellDesigner, PyBioS and SBML-PET) enable the use of 'events' in one way or another. Events evaluate a certain

condition (for example, whether simulation time has exceeded a certain threshold). If that condition is satisfied, a variable or parameter of the system is changed.

A straightforward approach is to set the concentration of an external input by an event. This results in a loss of steadiness of the time curves of the artificial input which causes numerical problems in the simulations.

To avoid this loss of steadiness, events are used to regulate the parameters of specially devised functions derived from the Hill-equation [35]. These functions regulate the increase or decrease of the concentration of the artificial inputs and are of the form:

$$\frac{dx}{dt} = S_1 \cdot k \cdot \frac{t^h}{\Theta_1^h + t^h} \; + \; (1 - S_1) \cdot k \cdot (1 - \frac{t^h}{\Theta_2^h + t^h}) \tag{1}$$

where t is simulation time in arbitrary units, h is the hill-coefficient. k specifies the maximal concentration of x (the maximal concentration also depends on the degradation term of x). Θ_1 and Θ_2 are equal to the value of t where x reaches its half-maximal concentration. Obviously, the function consists of two sumands. The first summand contains an 'activatory' Hill-equation that is growing with t, the second contains an 'inhibitory' Hill-equation that is declining if t is growing. Requiring $S_1 \; \varepsilon \; \{0, 1\}$, only one of the two sumands is not equal 0.

By switching S_1, an event can control whether the slope of the concentration is rising of falling while the simulation progresses. By changing Θ_1 or Θ_2, the onset of the rise or fall of the concentration is controlled. Variations in k lead to different maxima of the concentration of x

The values to witch these parameters are set must be chosen carefully to retain steadiness of the system.

When the parameter values are carefully chosen and multiple events are used to control one artificial input, complex time curves, for example the expression curve of *GataE* in Fig.18, can be mimicked.

4.1.3 Assumptions

The integration of new data into a model as complex as the proposed endomesoderm network poses a difficult task. Besides, the network itself is little more than an annotated directed graph. It is impossible to simulate the dynamic behavior of a system that is only described by a directed graph. Analysis of topological features is nevertheless possible. This lack of simulation spawns a vital question: Does the network, as depicted in Fig.9, adequately resemble the system's key interactions? This question is of utmost importance, since the integration of new data into a flawed model will certainly not result in a sensible model. Even more irritating, topological features derived from a flawed topology or common developmental mechanisms derived from a false model will obscure the true features and mechanisms.

To answer this vital question for the 'Endomesoderm Network' and design a working model of its well explored key components, I chose two parallel approaches. To infer the validity of the entire 'Endomesoderm Network', I constructed a model - hence called the endomesoderm model - of the entire network. To design a valid model for those parts of the network for which excessive data is available, I construct a smaller model, which is only loosely based on the Endomesoderm Network, called the core model. The name

core model is chosen because most of these well-explored genes belong to the 'core' of the network, i.e. a - expectedly - evolutionary conserved subnetwork that controls and initializes basic developmental steps in all deuterostomes [22].

Both the endomesoderm model and the core model are based on a few simplifying assumptions that limit the complexity of the model: No chromatin reorganization occurs in sea urchin embryos during the first 50 hours post fertilization and transcriptional regulation occurs only in the form of TF-binding mediated increase or decrease in transcriptional efficiency.

The first assumption is needed to employ time-invariant functions to model activatory and inhibitory strengths. The second assumption is used because the mechanisms underlying differential mRNA stability, splicing, mRNA interference and protein stability are generally not fully understood or quantified in the sea urchin and thus are not taken into account (except for β-catenin, where protein stability is regulated by the canonical Wnt-pathway).

The general approach employed in both models was to first construct a Boolean model based on the available data. The qualitative temporal expression pattern for the TFs regulating the transcription of each gene and the qualitative nature of each input (activatory or inhibitory) are given in [3]. The logical combination of these inputs that best reproduces the experimentally determined output of the gene (the assumed transcriptional activity) is chosen as the Boolean function controlling the state of the gene. Since perturbation data is very sparse (about 266 of 3969 theoretically possible [as the network contains about 63 genes, there are 63^2 pairwise interactions possible] interactions have been evaluated), it is not taken into account in the design step but rather in the validation of the model. The Boolean model here is generally designed and evaluated using spreadsheet software such as Gnumeric or OpenOffice.

The Boolean model is then automatically transformed to an SBML-compliant ODE model that is refined using SBML supporting software tools like Celldesigner [31].

Before I immerse into the details of the design of the two models, I summarize the rate equations used in the respective steps of the ODE models.

4.2 Kinetic Laws

The models employ rate laws to describe biochemical reactions. These rate laws generally follow mass action kinetics first described in [79].

The rate law determining the speed v_i of a reaction

$$X_i \xrightarrow{v_i} X_j \tag{2}$$

is - in the simplest case - of the form

$$v_i = k_i \cdot [X_i] \tag{3}$$

where $[X_i]$ denotes the concentration of substance X_i and k_i is a kinetic parameter.

If a backward reaction is necessary, i.e. the reaction is of the form

$$X_i \overset{v_i}{\underset{v_{-i}}{\rightleftharpoons}} X_j \tag{4}$$

, the speed of the forward and backward reaction are modeled using two rate laws:

$$v_i = k_i \cdot [X_i] \tag{5}$$

$$v_{-i} = k_{-i} \cdot [X_j] \tag{6}$$

Combining the rate laws that control the changes of a species' concentration yields:

$$\frac{d[X_i]}{dt} = v_{synth} - v_{degr} + v_{imp} - v_{exp} \tag{7}$$

where v_{synth} is the speed of the synthesis reaction for $[X_i]$, v_{deg} the speed of the degradation reaction and v_{imp} and v_{exp} are speeds of two transport reactions.

The most detailed model, as exemplified in Fig.8 has the following set of reactions:

- Protein degradation

$$v_{Protein-deg} = k_{Protein-deg} \cdot [Protein_{cytosol}] \tag{8}$$

- mRNA degradation

$$v_{mRNA-deg} = k_{mRNA-deg} \cdot [mRNA_{cytosol}] \tag{9}$$

- Nuclear transport (bidirectional)

$$v_{mRNA-export} = k_{mRNA-export} \cdot [mRNA_{nucleus}] \tag{10}$$

$$v_{mRNA-import} = k_{mRNA-import} \cdot [mRNA_{cytosol}] \tag{11}$$

$$v_{Protein-export} = k_{Protein-export} \cdot [Protein_{nucleus}] \tag{12}$$

$$v_{Protein-import} = k_{Protein-import} \cdot [Protein_{cytosol}] \tag{13}$$

- Transcription

$$v_{transcription} = k_{transcription} \cdot [Protein_{cytosol}] \tag{14}$$

The last equation concerning transcription is actually a placeholder. I will explain the details of the kinetics controlling transcriptional activation below.

Although biochemical networks generally depend heavily on the law of mass conservation, this network obviously does not satisfy the law. Assuming that mRNA is synthesized from single nucleotides and proteins are synthesized from single amino acids and that both single nucleotides and single amino acids are so excessively available that the modeled reactions do not significantly alter their concentrations (a gross simplification), it is permittable to exclude them from the above reactions.

Still, mRNA is not produced from nothing. Assuming a simplified model of transcription, a polymerase and the gene in addition to a TF act as enzymes catalyzing the reaction of many nucleotides to a strand of mRNA. When emitting the single nucleotides from the reaction, this will yield a new version for eq.14:

$$v_{transcription} = k_{transcription} \cdot [Protein_{nucleus}] \cdot [Polymerase] \tag{15}$$

The gene itself is omitted here. A similar approach is used to modify the other reactions, adding ribosomes for translation and similar species for degradation. If the concentration of the added species is constantly kept at 1 (arbitrary units assumed here), the result of the simple reactions remains unchanged (again assuming excessive concentrations of these catalysts).

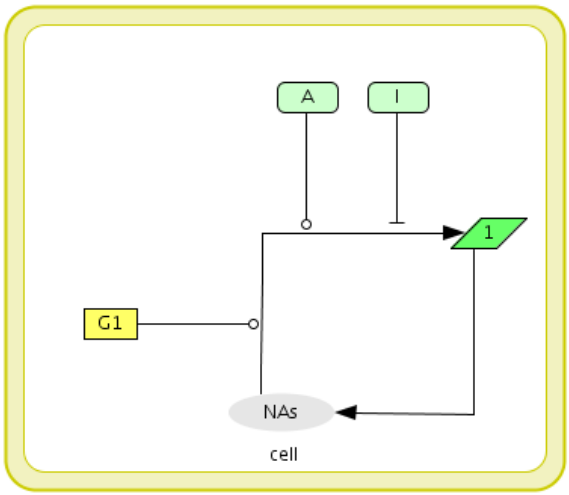

Figure 13: Topology of a simple GRN model. The expression of gene $G1$ is regulated by an activatory TF A and an inhibitory TF I. NAs represents the pool of nucleotides from which mRNA1 is synthesized.

4.3 Transcription

Different approaches have been used to realistically model transcriptional regulation by TF binding [8, 7, 9, 11, 69, 32, 71, 72]. Most of these approaches employ rather complex equations to realistically model the exact processes involved, such as binding kinetics between TFs and DNA, specificity of binding affinity and other mechanisms. For this work, in which a great number of regulatory interactions between TFs and genes has to be modelled, I propose a rather simple method to model transcriptional regulation by TF binding.

Generally a TF binds to a specific DNA-sequence motif and, by interaction with other sequence motifs, TFs or molecules involved in the transcriptional machinery inhibits or activates transcriptional activity. Regardless of the exact mechanisms, a TF must either have an inhibitory or activatory effect. The binding of a TF to a specific binding site depends on the binding specificity, affinity between TF and binding site and the TF concentration. Structural rearrangements of the genomic DNA can influence the affinity. Since specificity and affinity are both unknown for virtually all interactions in the model, they are emitted (assuming equality among these factors for all interactions). Thus, the binding of a TF solely depends on TF concentration in this model.

Once binding between TF and DNA-sequence is established, the strength of the activatory/inhibitory effects depends on the location of the TF, the nature of the TF and interactions between the bound TF and other TFs.

Assuming that there is only one binding site for each TF on a given gene (another gross simplification), the location of the TF binding and the nature of the TF are combined into one parameter.

I will construct two elementary formulas that will model an activatory or inhibitory influence of a TF on transcriptional activity. These two elementary formulas can be

combined in a modular manner so that interactions between multiple transcription factors are simple to model.

Thus, postponing the problem of interactions betwen TFs, the effect of a TF on transcriptional activity depends on the TF's concentration and one or more specific parameters.

For an activatory TF A, its influence on transcriptional activity, φ_{G_A}, on a given gene G is given by

$$\varphi_{G_A} = \frac{k_{A_G} \cdot [A]}{c_{A_G} + [A]} \tag{16}$$

where k_{A_G} is the parameter indicating the activatory strength of A and c_{A_G} is a threshold: If $[A]$ equals c_{A_G}, $\frac{[A]}{c_{A_G}+[A]} = 0.5$. As indicated by the notation, the parameters c_{i_j} and k_{i_j} are unique to each pair of TF and gene.

In the case of an inhibitory TF I, its influence on the transcriptional activity on gene G is defined as

$$\varphi_{G_I} = \frac{k_{I_G} \cdot c_{I_G}}{c_{I_G} + [I]} \tag{17}$$

with parameters defined analogously to above. In case the absence of the inhibitor results in some kind of default activity of the gene, $k_{I_G} > 1$, in the case that there is no default activity in absence of the inhibitor, $k_{I_G} = 1$. In both cases, repression of the gene's activity will occur when $[I]$ significantly exceeds the threshold c_{I_G}.

Any number of these two elemental formulas may be combined using addition or multiplication. Logical OR is transferred to addition of atomic formulas, since the presence of any of the involved factors will have an effect. Multiplication here corresponds to a logical AND in a Boolean model. Only when all TFs involved in the multiplication are present, a regulatory change will occur.

Notice that theoretically, multiplication is not the continuous equivalent of logical AND. Here, the choice of parameters is used to adapt the function to behave as desired, although these parameters need not necessarily directly correspond to measurable chemical constants like kd values.

To exemplify these combinations, consider a network like the one depicted in Fig.13, in which the transcriptional activity is controlled by two TFs. One of these TFs has an activatory effect, the other one an inhibitory. There are exactly two possible combinations of the two inputs to the gene: Either the activator must be present AND the inhibitor must be absent or the activator must be present OR the inhibitor must be absent (this OR is not exclusive, the overall condition is also satisfied if both individual conditions are satisfied). The two possibilities result in a total transcriptional activity φ_G of the gene G

$$\varphi_G = \frac{k_{A_G} \cdot [A]}{c_{A_G} + [A]} \cdot \frac{k_{I_G} \cdot c_{I_G}}{c_{I_G} + [I]} \tag{18}$$

for the AND-case. The OR-case is given by

$$\varphi_G = \frac{k_{A_G} \cdot [A]}{c_{A_G} + [A]} + \frac{k_{I_G} \cdot c_{I_G}}{c_{I_G} + [I]} \tag{19}$$

The expression that results from these two different combinations is depicted in Fig.14.

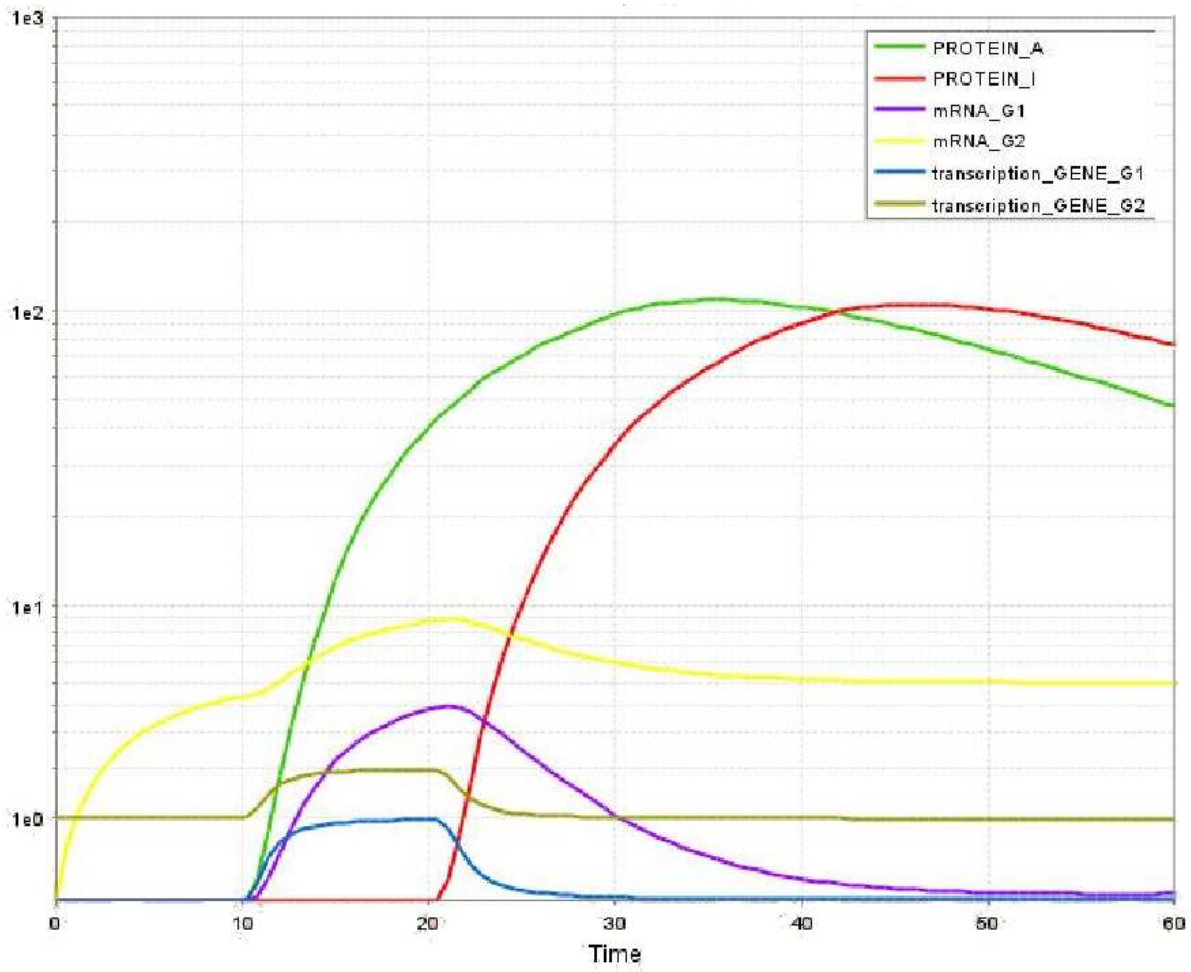

Figure 14: Simulation results of a model resembling the topology shown in Fig.13. Note that the y-axis has a logarithmic scale. Different scales are combined on the y-axis: For proteins and mRNA, the concentration in absolute numbers is used while reaction rates ($transcription\_GENE\_G1$ and $transcription\_GENE\_G1$) are measured in $\frac{absolute\ numbers}{time\ in\ arbitrary\ units}$ Two genes are expressed here,both have a positive and a negative input. The amount of transcripts for gene $G1$ is depicted as $mRNA\_G1$, the number of transcripts for $G2$ likewise as $mRNA\_G2$. The number of TFs is depicted by $PROTEIN\_A$ and $PROTEIN\_I$. $transcription\_GENE\_G1$ and $transcription\_GENE\_G2$ show the transcriptional activity for $G1$ and G2, respectively. For gene G1 these inputs are combined using multiplication/logical AND (see eq.18), for gene G2 the inputs are combined via addition/logical OR (see eq.19). All parameters involved in the regulation of the genes are equal for both genes. The simulations were carried out using CellDesigner3.2.

When choosing the right parameters, this algorithm enables easy transfer of a Boolean model of a GRN to an ODE model.

I would like to stress the point that the parameters that enable the reproduction of experimental data with this algorithm need not necessarily be realistic parameters (as, for example, the dissociation constant between a TF and the corresponding sequence motif). These realistic values are generally unknown and extremely difficult to determine by experimental methods. Furthermore, the integration of these simple kinetics reduces the computational demands of simulation runs and enhances legibility of the model. Thus, their use is justified here.

4.4 Modeling of the Endomesoderm Model

As explained before, the network proposed by Davidson et al. (Fig.9) is - as a model - not capable of simulation and thus not suited for validation. Therefore, I constructed an ODE model from the network topology, using the assumptions and kinetics as described above. The model will thus feature one cell that emits three different expression patterns based on the external inputs.

Although the network does not explicitly describe the way in which the different inputs of a gene are to be combined, some publications imply an all-AND or all-OR combination of most genes (see [73] for an example). Due to the complex expression patterns that are to emerge, I refrain from this approach and rather use the qualitative expression data as given in [3] to construct a sensible model.

After designing a sensible Boolean model of the large network, it is automatically transferred to an ODE model. The script for the conversion of the network (the resulting SBML-file still needs minor corrections) and sample input is explained in the supplemental information.

The model is sensible only in considering the qualitative input to each gene related to the qualitative output of the gene as shown in [3]. The topology is not verified in the course of modeling. This model is rather used to infer the validity of the topology as explained in the results section.

This ODE model consists of 290 species in three compartments, the outside, the cytosol and the nucleus. The species interact via 432 reactions which contain 230 parameters. For the SBML-Code of the model, see the supplemental information.

The general parameters that apply equally to all different species of the same kind are chosen as follows: $k_{translation} = 2.0$, $k_{mRNA\_deg} = 0.2$, $k_{protein\_deg} = 0.05$, $k_{transport} = 0.4$.

The artificial inputs that drive specification of the cell types were obtained from [3]. Used are those components of the network that are independent from other components and differ for which activation is assumed to differ between the cell types: *UbiqES*, *UbiqHnf6*, *UbiqRofMic* and *UbiqSoxB1*.

4.5 Modeling of the Core Model

This model is based on an approach contrary to that of the endomesoderm model. As the endomesoderm model is used to test whether the underlying topology can reproduce the experimental data (the accordance between the data and the resulting model, given

that the simplifying assumptions are valid), the core model is a new model with its own topology that is optimized to best reproduce the experimental results.

Because this model is later subjected to parameter estimation, its complexity was reduced by omitting intracellular compartimentation.

The first step, again, is the construction of a Boolean model. This model consists of only 16 dependend species. Based on the qualitative information in [3] and the experimentally established interactions (see, for example [85]) a Boolean model with a topology similar to that of the network is constructed. Since the experimental data is not nearly reproduced with this network, especially not the establishment of the three cell-type specific expression patterns, the network is refined.

This refinement includes the integration of new input variables, rewiring of the edges and corresponding alterations to the logical formulas as well as subsequent elimination of those input variables that can be exchanged for one or a combination of multiple dependant variables.

This elimination process can very well lead into dead ends, but it also simplifies the model and proposes new interactions for experimentally verification.

The resulting network topology is depicted in Fig.15 and the Boolean functions are given in the supplemental information.

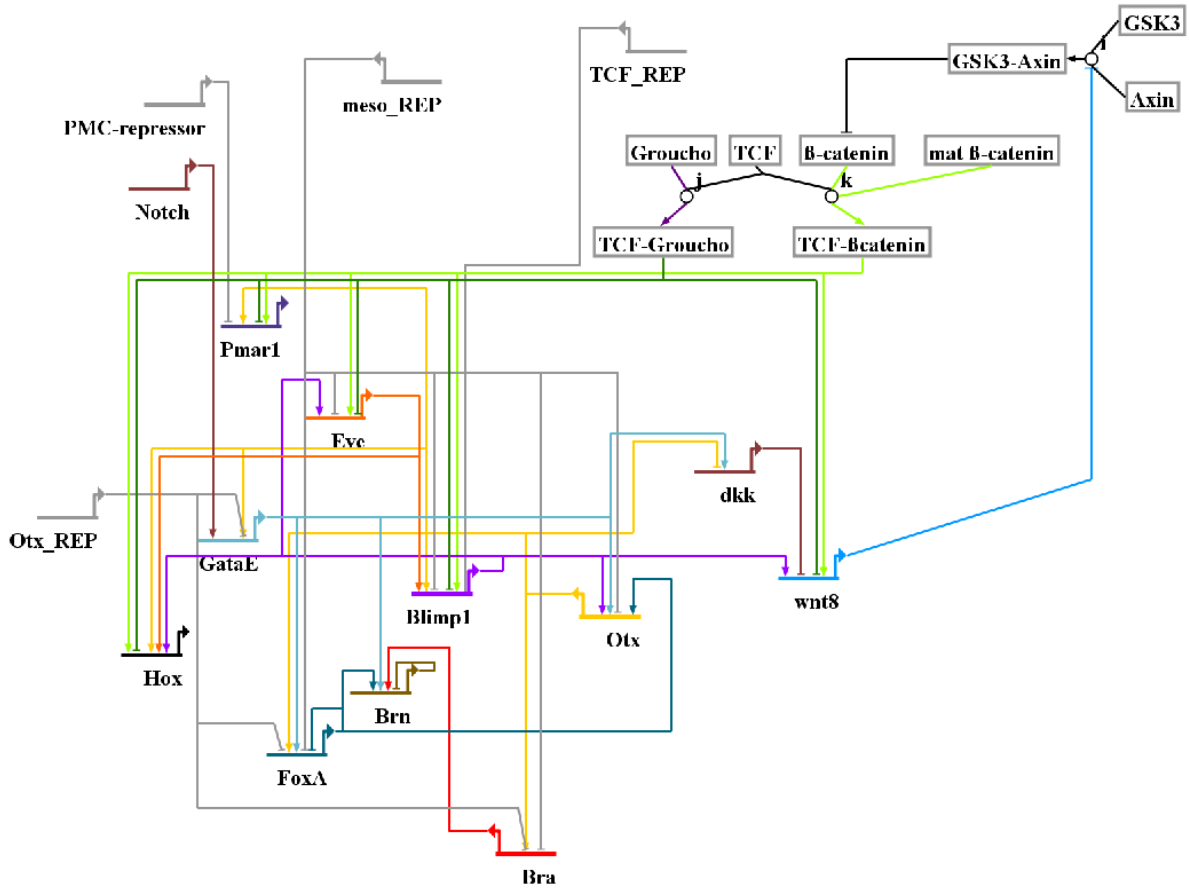

Figure 15: Topology of the Boolean core model, created using BioTapestry [56]

The developed Boolean model is then transferred into an ODE model, using the same procedure as with the endomesoderm model. This ODE model is used to estimate parameters that reproduce the calculated cellular expression data and the differences of the three cell types.

In the core model, as opposed to the network diagram and the endomesoderm model, the Wnt-pathway is accredited as a key pathway starting endomesoderm specification. This model is thus partly based on [48, 50]. Although this model of the Wnt-pathway could not be directly applied, its basic features have been conserved to guide in the establishment of the bistability of the canonical Wnt-pathway here.

The results of *in-silico* perturbation experiments using the estimated parameters can be compared to results of the same experiments using sampled parameters. This allows for a rough inference of the applicability of the M-C approach since sensible parameters are being estimated here.

The general parameters that apply equally to all different species of the same kind are chosen as follows: $k_{translation} = 2.0$, $k_{mRNA\_deg} = 0.2$, $k_{protein\_deg} = 0.10193$ (so that mRNA halflife is $\frac{1}{2}\cdot$ Protein halflife), $k_{transport}$ is not applicable since compartimentation is omitted.

Artificial inputs to the model were determined either from experimental data [3] or necessity in the Boolean model. The artificial inputs are: TCF-repressor (active $24-50\ hpf$ in endoderm), Notch (active $21-50\ hpf$ in endoderm and PMC, $12-50\ hpf$ in mesoderm), PMC-repressor (active in endoderm and mesoderm throughout the simulation), Otx-repressor (active from simulation start to 14 hpf in endoderm, simulation start to 17 hpf in mesoderm and simulation start to 10 hpf in PMC) and mesoderm-repressor (active $15-50\ hpf$ in mesoderm and $9-50\ hpf$ in PMC)

5 Monte-Carlo Topological Verification

To infer dynamical properties of an ODE model in which most of the parameters are unknown, as is the case with the endomesoderm model, I chose an approach using Monte-Carlo Methods. Although topological features are tangible by the analysis of directed graphs or Boolean models, this approach could possibly generate more detailed information.

In this approach, a large number of parameter sets is sampled from a reasonable random distribution. Simulations are computed for each parameter set.

General properties of a model are expected to be generally invariant to parameter changes, thus the main properties should be detectable as similarities in all simulations.

To validate the endomesoderm model, experimental data from perturbation experiments as well as temporal expression data is available.

As mentioned before, the reproduction of the exact temporal expression data is difficult to achieve with a single cell model. Furthermore, certain obvious flaws in the actual version of the Endomesoderm Network hint to an inability of the network in generating the exact expression patterns. For example, Otx is - in mesoderm and PMC cells - known to be turned off at a certain time point. In the network, Otx has no negative input but is part of a positive loop both with itself and with Blimp1 (see Fig.9). One of the features of the network topology depicted in Fig.9 is that Otx transcriptional activity is impossible

to shut down once it is activated (compare Fig.8).

To analyze whether the network can at least correctly reproduce the perturbation experiments which it is based on, I use the Monte-Carlo approach in the following way.

After a reasonable ODE model of the network had been constructed, this model was imported into PyBioS [83], an environment for the modeling of biochemical systems based on python and exported again for computation.

This exported version ships with numerous python programs that allow for sampling of parameters, simulation of models and analysis of results.

The PyBioS code was used to generate a large number of parameter sets for the model. The kinetic parameters that control transcriptional regulation were sampled from a lognormal distribution ($\mu = 1.5, \sigma^2 = 0.5$). All other parameters are equal among all parameter sets.

Different versions of the basic exported model (which had to be slightly revised to retain the artificial inputs) were constructed. Each of these versions features the KO (knock-out) of a single gene.

Each of the different KO models and the unperturbed model were simulated for all parameter sets using an automated pipeline from PyBioS.

The result of these simulations were analyzed with modified version of the original PyBioS code.

This statistical analysis compares the result of simulations under one specific KO condition to the simulation results under unperturbed conditions. Different results emerge from simulations employing different parameter sets. All successfully finished simulation runs of the KO condition in question matching finished simulation runs under unperturbed conditions are considered, giving rise to two paired sets of simulation results, KO and $CONTROL$. Both KO and $CONTROL$ consist of n result sets obtained from n parameter sets. KO_i and $CONTROL_i$ each consist of the simulated concentrations of mRNAs $mRNA_1$ to $mRNA_m$.

To asses the effect of a KO on the concentration of $mRNA_j$ at time point t, all values of KO and $Control$ pertaining to $mRNA_i$ and t need to be considered, namely exp and ctl, which consist of $KO_{1\ mRNA_j}...KO_{n\ mRNA_j}$ and $CONTROL_{1\ mRNA_j}...CONTROL_{n\ mRNA_j}$, respectively.

exp and ctl can be compared in various ways. The possibly simplest is by computing the ratio $R_m = \frac{E(exp)}{E(ctl)}$. This method might become inapplicable when the variances of exp or ctl are greater than their respective means and also disregards the information of the paired values.

To include this pairing information in the analysis, it is possible to calculate the mean of all pairwise ratios as

$$M_p = E(\frac{exp_1}{ctl_1}, \frac{exp_2}{ctl_2}, ..., \frac{exp_n}{ctl_n}) \tag{20}$$

This method is still vulnerable to great variances.

A method based on the calculation of the pairwise ratios is to count whether a certain fraction of these ratios is above or below a certain threshold. In this application, this method is used in two versions: T_1 indicates whether at least 90% of the pairwise ratios $\frac{exp_1}{ctl_1}, \frac{exp_2}{ctl_2}, ..., \frac{exp_n}{ctl_n}$ are greater than 1.5 or less than 0.75. T_2 is used to detect less significant effects and therefore requires only 80% of the pairwise ratios to be greater than 1.1 or less than 0.9 to detect an effect.

Statistical tests can also be employed to compare the two lists of samples *exp* and *ctl*: If the values in both lists can be assumed to originate from a normal distribution, the student's t-test (first used in [34]) can be used. If normality can not be assumed, non-parametric test must be used. Here, the Kolmogorv-Smirnov test [24] and the Wilcoxon signed-rank test for paired values [84] are employed.

A scatterplot can visualize the difference emerging between control and knock-out conditions. In a scatterplot, paired values (*exp* and *ctl* here) are visualized by plotting the paired values in a coordinate system given by the values of one element (*ctl*) of a pair on the y- and the other element (*exp*) on the x-axis. If all points are on the straight line $f(x) = x$, no differences between *exp* and *ctl* arose. If the points are mostly above the line, a significant negative influence of the KO on the plotted species is assumed. If the points are mostly below the line, a significant positive influence of the KO is assumed.

6 Results

6.1 Results of the Core Model

6.1.1 Model Construction and Parameter Estimation

The final topology of the ODE core model is shown in Fig.15. This version is the result of constant refinement but nevertheless far from finished.

The first model already contains new data from [1] in the form of *Dkk* which inhibits *Wnt* expression. The first refinement was performed on the Boolean model to improve reproduction of the experimental data while complying to biological constraints. The next step was to substitute artificially set inputs like the activity of *Dkk* for dependencies on other constituents of the model. This was performed by comparing dependend gene's activity to that of artificially set genes. Most of the interactions thus inferred have to be validated by experimental methods.

The last refinement was performed on the ODE model. After the parameters had been estimated to reproduce the experimental data, some features of the experimental data could not be reproduced. One of these features that could be resolved is the expression of *Brn*. To resolve it, the ODE model was reduced to a simpler version that is still able to reproduce the data. The parameters and kinetics involving regulation of *Brn* transcription have then been tuned by hand and the simulation results could be improved in regard to reproduction of the experimental expression time curves. The improvement could be carried over to the full model.

When investigating the Boolean and the ODE version of the core model and their capability to reproduce the respective experimental data, one has to keep in mind that the experimental data differs in each case: The Boolean core model is based on the qualitative data as given in [3], which is probably inferred from the raw transcript numbers per embryo. The ODE version of the ore model, on the other hand, uses the refined data of transcripts per cell expressing, as described in section 3.2.

After a reasonable Boolean model had been established, it was transferred to an ODE model in SBML syntax. This ODE model was - after refinement - used to perform parameter optimization using SBML-PET [87]. SBML-PET takes an ODE model in SBML syntax and a file containing the parameters to be estimated along with experimental time

courses as input.

In the first attempt to estimate the parameters for the core model, the entire model was used. Due to the complexity of the parameter estimation and the numerous dependencies between the parameters, the runtime of this approach was intolerable. Even worse, the first results were not capable of generating different expression patterns for the three cell types.

One solution to this problem is to construt a model that contains three copies of the core model using different inputs but the same parameters to simulate the three cell types in parallel. Since the runtime of SBML-PET using a model containing only one copy of the core model is unsatisfying, this approach is obviously inapplicable here.

Because experimental temporal expression curves are available for all genes in the core model, it is possible to partition the model into a set of models with only one dependend gene. The inputs of the gene in question are approximated combining activatory and inhibitory Hill-Kinetics (first developed in [35]) that mimic the experimental data for the transcription of the genes that constitute the input of the dependend gene. The only problem that arises with this approach is the identification of exact parameters for the Wnt-pathway. But by hand-tuning the results of a first estimation thereof, a reasonable set of parameters for the canonical Wnt-pathway could be obtained. One problem concerning the applicability of the model of the canonical Wnt-pathway here is that no experimental data concerning the *TCF*, *β-catenin* or *Groucho* transcript or protein numbers could be included. Publications suggest a transcriptional regulation of these key components of the pathway by the pathways activity itself (TCF for example [41]). Thus, the implementation of the canonical Wnt-pathway employed here is only a rudimentary approach that needs refinement. The partitioning of the core model as used for parameter estimation is shown in Fig.16.

After sensible parameters were estimated for each submodel, the submodels were combined again to form the original core model. A model containing three copies of the core model with estimated parameters was used to generate simulation results for the three cell types in parallel. As described above, this model was refined again and the simulation results of this refined core model with estimated parameters are shown in Fig.17.

For comparison, the experimental data for each gene, recalculated to $\frac{transcripts}{cell\_expressing}$ is depicted in Fig.18.

Comparing the simulation results from Fig.17 with the experimental data in Fig.18, accordances between simulation and experimental results are apparent. The curves of the simulation results often mimic the curves of the experimental measurements. In cases where the match between simulation and experimental data is not apparent, the qualitative features of the experimental data are nevertheless reproduced.

6.1.2 Simulation Results and Comparison to Experimental Data

Experimental data suggests expression of *Blimp1* in endoderm cells with a peak at 12 *hpf* of 31.25 transcripts per endoderm cell. It rapidly declines to a lower level of expression between 10 and 20 transcripts per cell until about 40 *hpf* and then falls to 0. This temporal behavior is roughly reproduced by the simulation results in Fig.17: The expression rises sharply in all cell types (up to almost 25 in endoderm and 22 to 18 for mesoderm and

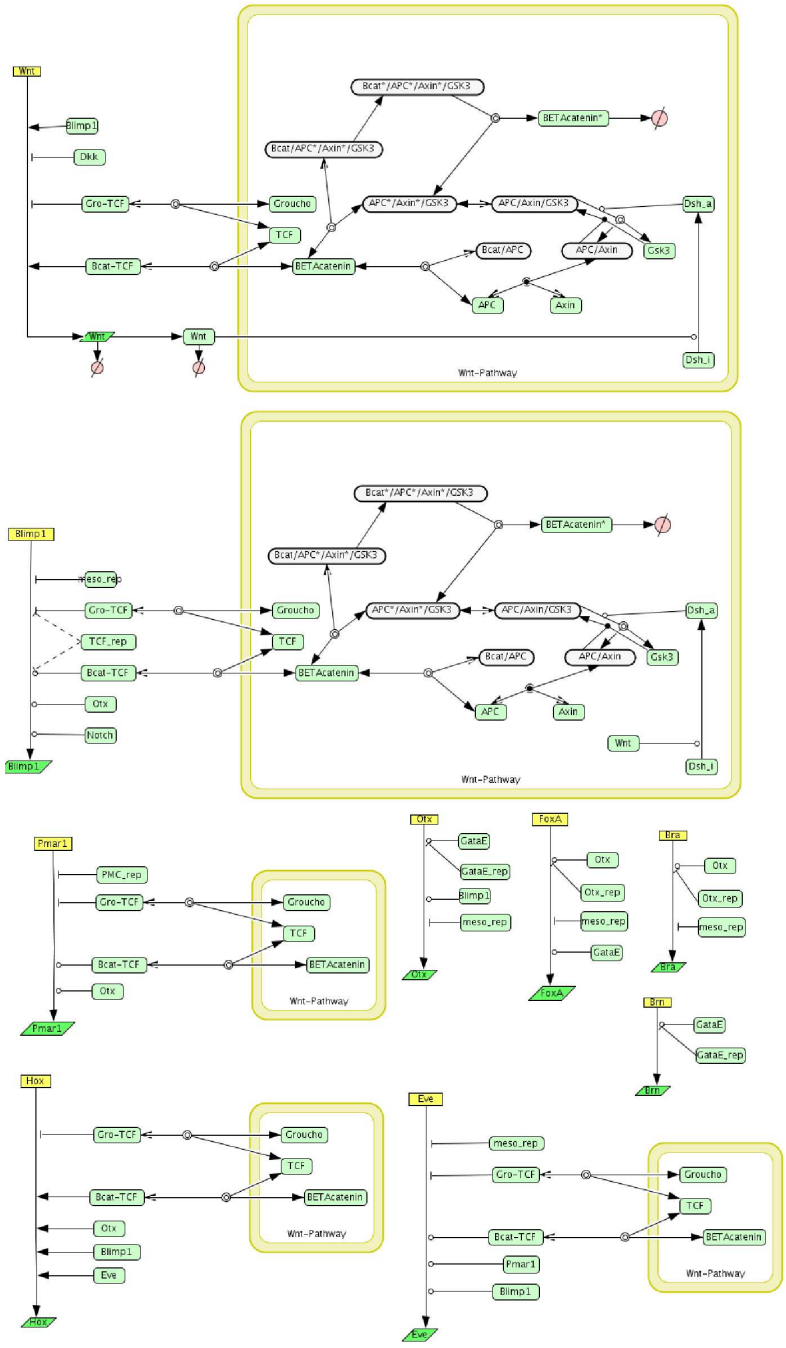

Figure 16: Topology of the submodels of the core model as used for parameter estimation. Each rectangular box represents a gene, trapezoids are the corresponding mRNA and the arrow from gene to mRNA represents the transcription. Activatory (lines with circles at the end) and inhibitory (lines with bars at the end) inputs to the respective transcription are shown. The concentration of the TFs (ovals) were controlled to resemble experimental data. The parameters of the Wnt-pathway were also estimated during the estimation of parameters for *Wnt* transcription. With minor adjustments, the Wnt-pathway was included where necessary as shown in the *Blimp1*-subnetwork.

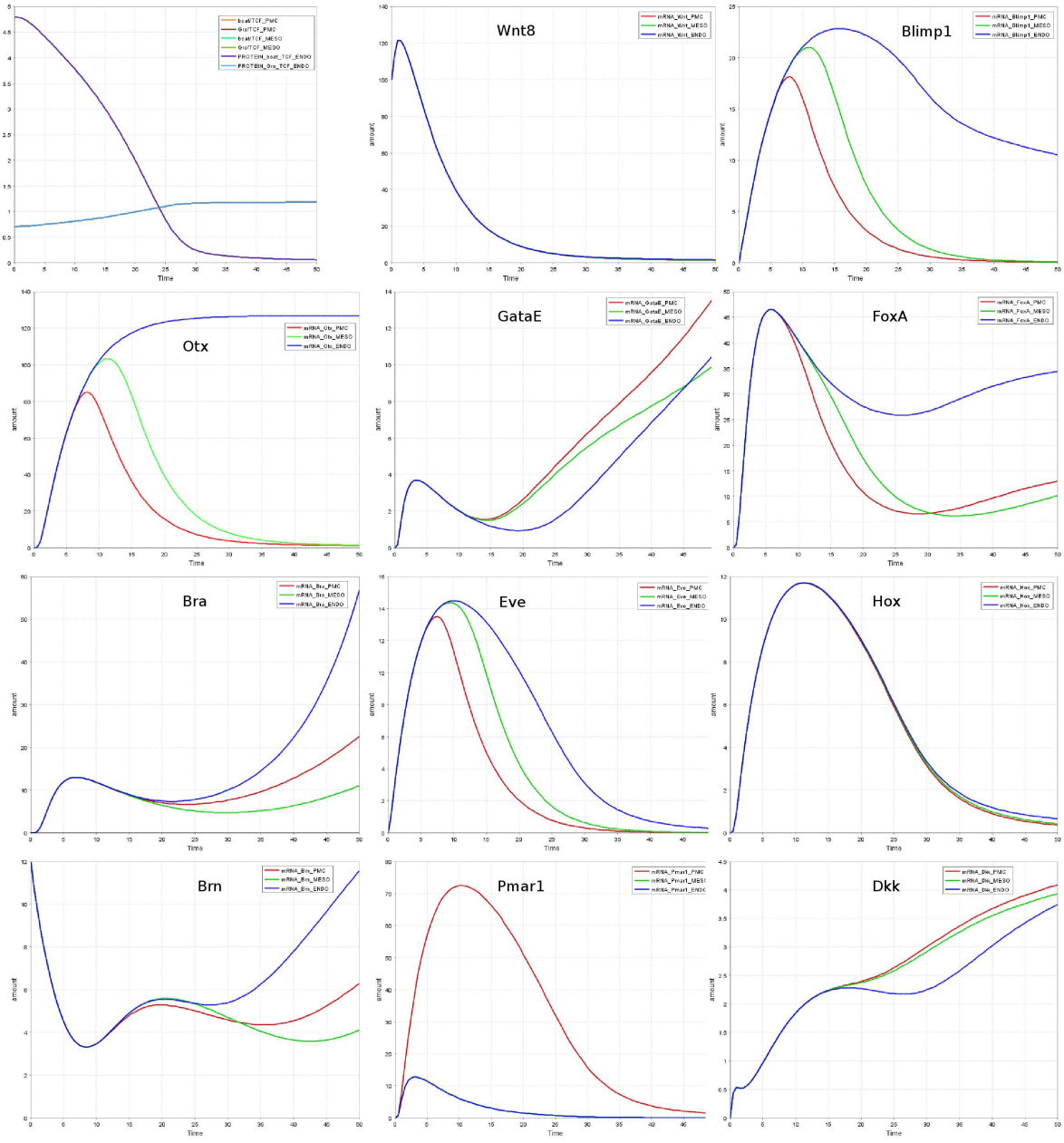

Figure 17: Simulation results of the final version of the core model. The topology of the underlying network is given in Fig.15. Each panel shows the expression of one gene in the three different cell types(endodermal expression in blue, mesodermal expression in green and PMC expression in red) as absolute numbers of mRNA. The upper left panel depicts concentrations of the protein complexes TCF/Groucho (lighter blue) and TCF/β-catenin. The x-axis depicts hpf, the y-axis absolute transcript numbers per cell. Note that some curves might overlap, so that underlying are not visible anymore (this is the case with *Wnt8*, TCF/β-catenin and TCF/Groucho, where all three territories exhibit the same behavior and *Pmar1*, where endodermal and mesodermal expression overlaps). Simulations were performed using CellDesigner3.2.

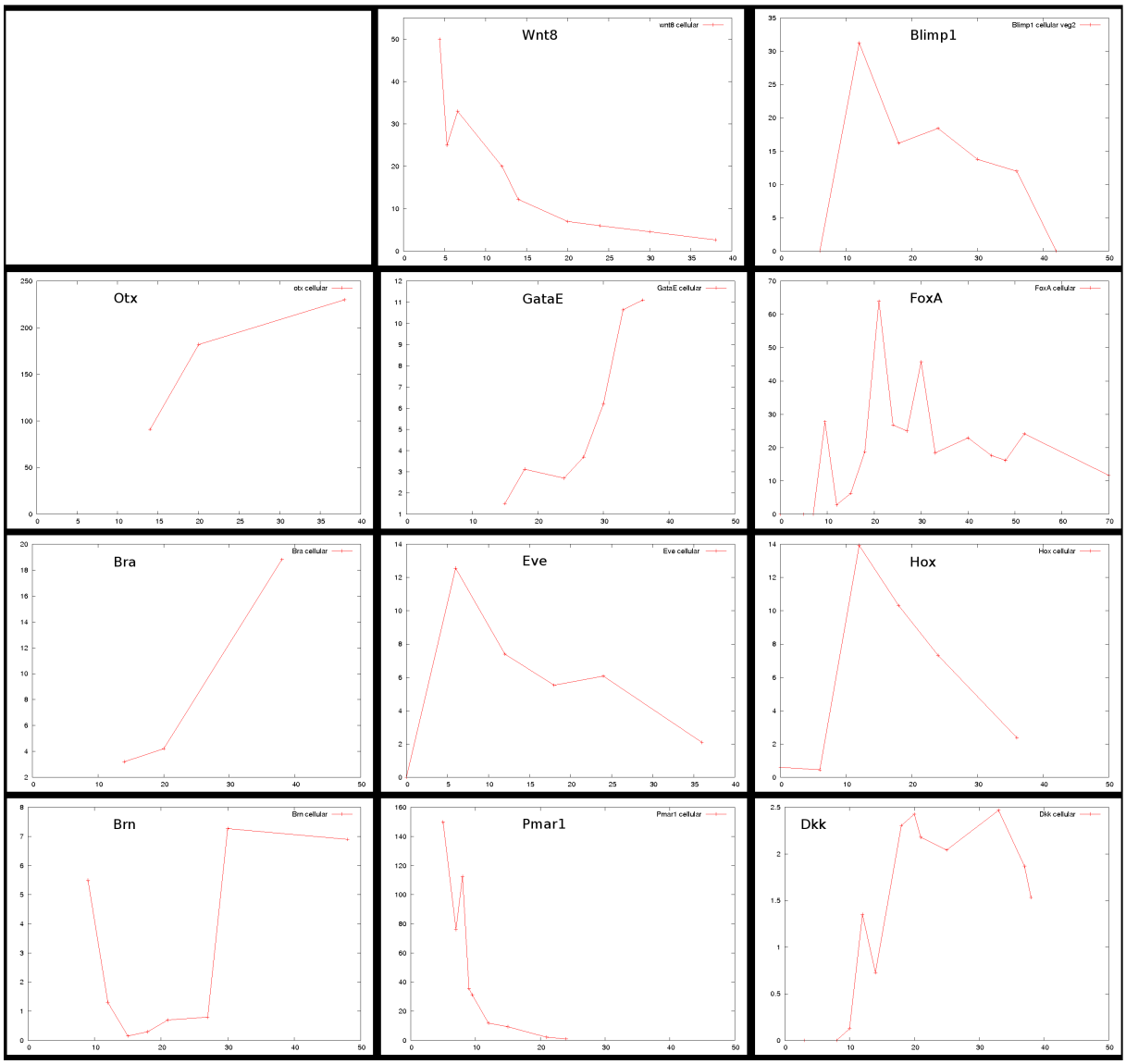

Figure 18: Experimentally determined gene expression for each Gene of the core model, recalculated as described in section 3.2. The x-axis indicates hpf, the y-axis indicates absolute transcript numbers per cell expressing the given gene. TCF/β-catenin and TCF/Groucho are not shown since no experimental data exists.

PMC cells) and then declines to 0. Endodermal expression is sustained and declines only to about 10 transcripts per cells. Endodermal expression does not fall below 10 transcripts per cell, but that might be an effect of slight shifts on the time scale.

Brn has a very distinct temporal expression profile. The number of transcripts falls from a suspected 12 transcripts/cell at fertilization to almost none at 15 hpf. At about 28 hpf, the expression sharply rises to about 7 transcripts per cell. Again, expression is mainly confined to endodermal cells. The simulation results fail to quantitatively reproduce the experimental data but the qualitative changes of transcript numbers and the spatial confinement of *Brn* expression is reproduced.

The recalculated expression pattern of *Wnt8* is reproduced very closely. From an expected initial concentration of about 120 transcripts directly after fertilization, the number of transcripts falls in an exponential manner.

The experimentally determined expression of *Pmar1* declines from 150 transcripts per PMC cell at 5 hpf. At 10 hpf, the number of transcripts per cell is already dropped to about 20. For the simulation results, an initial concentration of 0 transcripts was chosen. Thus, the number of transcripts rises sharply in PMC cells to about 73 transcripts per cell at 10 hpf and then declines again. Although the exact temporal expression pattern is shifted again, the simulation results lead to the same qualitative results, especially concerning the spatial confinement of expression.

As with *Brn*, *Wnt8* and most other genes in the core model, there are no measurements of transcript numbers in the fertilized egg (or early stages of development before 5 hpf) available for *Pmar1*. It is therefore not determinable whether the spatiotemporal expression patterns of some genes do result from unequal cleavages where the nuclear complement of TFs or mRNA is changed.

The experimental data of *Bra* expression is exceptionally sparse but is observed to rise sharply from about 15 hpf on. *Bra* expression is confined to endodermal territories and is thought not to be expressed in the early endoderm [13]. The simulation results show significant expression in the early endoderm, and a strong rise in expression from about 30 hpf on, especially in endoderm.

The expression of *Dkk*, as experimentally determined, rises from about 10 hpf on to a level of about 2.3 transcripts per cell, a level that is sustained until 35 hpf, from whereon it declines again. *Dkk* expression is considered to be confined to mesodermal territories. Since in the core model, it is used as an ubiquitous inhibitor of *Wnt* activity, the expression in the core model is not confined to a specific territory. It rises to a level of 0.5 transcripts per cell at the very beginning of the simulation and then more or less continuously rises to about 4 transcripts per cell. The simulation results thus not reproduce the experimental data. Since there are no publications concerning the regulation of *Dkk* available yet, this part of the model is only a basic attempt to include new data. Furthermore, I must denote that Dkk is not really a TF that inhibits Wnt expression but rather an extracellular molecule that inhibits the binding of extracellular Wnt8 to the Dishevelled receptor. Thus, this part of the model clearly needs refinement, focusing on the canonical Wnt-pathway and extracellular gradients (of *Dkk*) again.

Eve transcription, as experimental data indicates, rises from 0 transcripts at fertilization to a maximum of about 12 transcripts per cell at 6 hpf and then sharply declines to about 6 transcripts per cell. It gradually sinks from about 25 hpf on. The simulation results show a strong rise to about 14 transcripts per cell at about 10 hpf. It then rapidly

declines, not exhibiting the low level of transcription as in the experimental data. Experimental data indicates *Eve* expression in endomesoderm up to 12 *hpf* and in endoderm at later stages of development. The simulation results show *Eve* expression in all three cell types, although PMC expression is weakest and shortest while Endodermal expression is stronger and significantly longer lasting.

The experimentally determined expression of *GataE* rises to about 3 transcripts per cell, where it remains from about 18 to 25 *hpf*, and then rises steeply to about 12 transcripts per cell at 35 *hpf*. The experimental data does not indicate whether it rises, falls or remains stable after 35 *hpf*. In the simulation results, *GataE* expression rises to about 3 transcripts per embryo at 4 *hpf*, declines slightly and then rises from about 20 *hpf* on and reaches 10 - 14 transcripts per embryo at 50 *hpf*. Although experimental data shows that *GataE* is clearly expressed in endodermal and mesodermal territories only, the simulation results show the strongest expression for PMC cells, where no endogenous expression at all is observed in experiments.

Hox is shown to be expressed in endoderm and mesoderm. Initially, it remains at low transcript numbers, then rises sharply from 6 *hpf* on to almost 14 transcripts per cell at 12 *hpf* and then declines to about 2 transcripts per cell at 36 *hpf*. The simulation results do not exhibit the low initial transcription but show a direct rise resulting in almost 12 transcripts per cell at about 11 *hpf* and then an exponential decline, leaving only 2 transcripts per embryo at about 34 *hpf*. Although this temporal expression is very close to the experimentally determined values, the spatial confinement could not be reproduced but all three cell types' simulations exhibit an equal expression pattern.

Experimental data for *Otx* is again exceptionally sparse. Only three time points have been obtained, showing a rise from about 80 transcripts per cell at 14 *hpf* to 220 transcripts per cell at 38 *hpf*. Otx is assumed to be expressed in endoderm and mesoderm, mesodermal expression is shut down at 18 *hpf*. The simulation results show an increase from initially 0 transcripts to about 120 transcripts per cell, where endodermal expression remains from about 20 *hpf* on. Mesodermal expression only rises to about 105 transcripts per cell at 12 *hpf* before it decreases again. PMC expression rises to about 80 transcripts per cell at 6 *hpf* and then declines.

The experimentally determined expression of *FoxA* exhibits an oscillatory pattern: The number of transcripts per cell rises to 28 at 9 *hpf*, declines to almost none at 12 *hpf*, then rises to over 60 at 21 *hpf*, falls to less than 30 at 24 *hpf*, rises to over 40 at 30 *hpf*, falls to about 20 at 33 *hpf* and then remains - with minor oscillations - at about 20 transcripts per cell up to 50 *hpf* from where on it slowly declines. The simulation results reproduce the initial rise in *FoxA* expression in all cell types. Mesodermal and PMC expression is then shut down while endodermal expression declines and then rises again, reproducing the spatial restriction to endodermal territories as determined in experiments.

6.1.3 Perturbation Experiments using Estimated Parameters

To further validate the core model, perturbation data [3] was considered. The model was simulated with genes knocked out to compare the results with those of the MASO (Morpholino-substituted antisense oligo nucleotide) experiments. To knock a gene out in the model, its normal transcriptional activity was reduced by 95%. Only *Blimp1*, *Eve*, *FoxA*, *GataE* and *Otx* were knocked out since the other gene's expression either has no

effect in the model or there is no comparable experimental data.

The results of these perturbed simulations are exemplified in Fig.19, which depicts the simulation results of *Blimp1* knock-out.

Although one can estimate qualitative effects of knock-outs from the results as depicted in Fig.19, a quantitative assessment of the effects is rather difficult. To quantify the regulatory effects, I computed the ratio of transcript numbers of the effected genes under normal and knock-out conditions. This quantification is depicted in Fig.20.

Using Fig.20, the effects of the simulated knock-outs are easily accessible: *Eve* and *FoxA* knock-outs have the least effect. While *Eve* knock-out only slightly decreases the number of *Blimp1* transcripts, *FoxA* knock-out leads to a strong reduction of *Brn* transcript numbers and a slight drop in *Bra* and *Otx* expression.

The knock-out of *Blimp1* and *Otx* each leads to a decrease in transcriptional activity for most genes of the network: Knocking out *Blimp1* leads to a slight reduction of *Bra*, *Brn*, *Dkk* and *GataE* transcriptional activity. Medium to strong descents in transcriptional activity are detectable for *Eve*, *Hox*, *Otx*, *Pmar1* and *Wnt8*.

When *Otx* is knocked out, the simulations reveal slight decline in transcript numbers for *FoxA*, *Eve*, *GataE* and *Hox*. A medium decrease in transcriptional activity is detected for *Dkk* and *Pmar1*. A strong reduction of transcript numbers is measured for *Bra* and *Brn* transcripts. *Wnt8* transcriptional activity sinks up to 19 hpf and is slightly increased from 25 hpf on.

Wnt8, along with *Blimp1*, *Eve*, *Hox* and *Pmar1*, is also stronger expressed if *GataE* is knocked out. Meanwhile, *Otx* expression is slightly dampened and *Brn*, *Dkk* and *GataE* expression is strongly decreased.

As seen in Fig.20, all effects are detectable in all three cell types, though they vary considerably in strength and duration between the cell types.

These findings will later be compared to the experimental data of analogous experiments as depicted in Fig.21.

6.1.4 Perturbation Experiments using Sampled Parameters

500 different parameter sets were sampled for the core model, using a lognorm distribution with $\mu = 1.5$ and $\sigma^2 = 0.5$. Only parameters concerning transcriptional regulation were sampled. Parameters controlling degradation of species or translation and the parameters involved in the regulation of the canonical Wnt-pathway were retained as in the original model. Using these parameter sets, 500 different simulations for each knock-out mentioned above and the unperturbed model were computed. The methods described in section 5 were applied to analyze the results.

Since the distribution of the simulation results (transcript numbers for a gene at a certain timepoint) of all parameter sets can in general not be approximated by a normal distribution (see Fig.22 for an example), the student's t-test could not be applied in the analysis of the results.

Thus, only the ratio of the means , R_m, of the simulation results under control and knock-out conditions, the mean of the paired values, M_p, computation of $T1$ and $T2$, the Wilcoxon signed rank test, W, and the Kolmogorov-Smirnov test, $K - S$, were applied to the results. For details of the applied methods, see section 5.

The results show that in most cases, there is no significant difference between R_m and

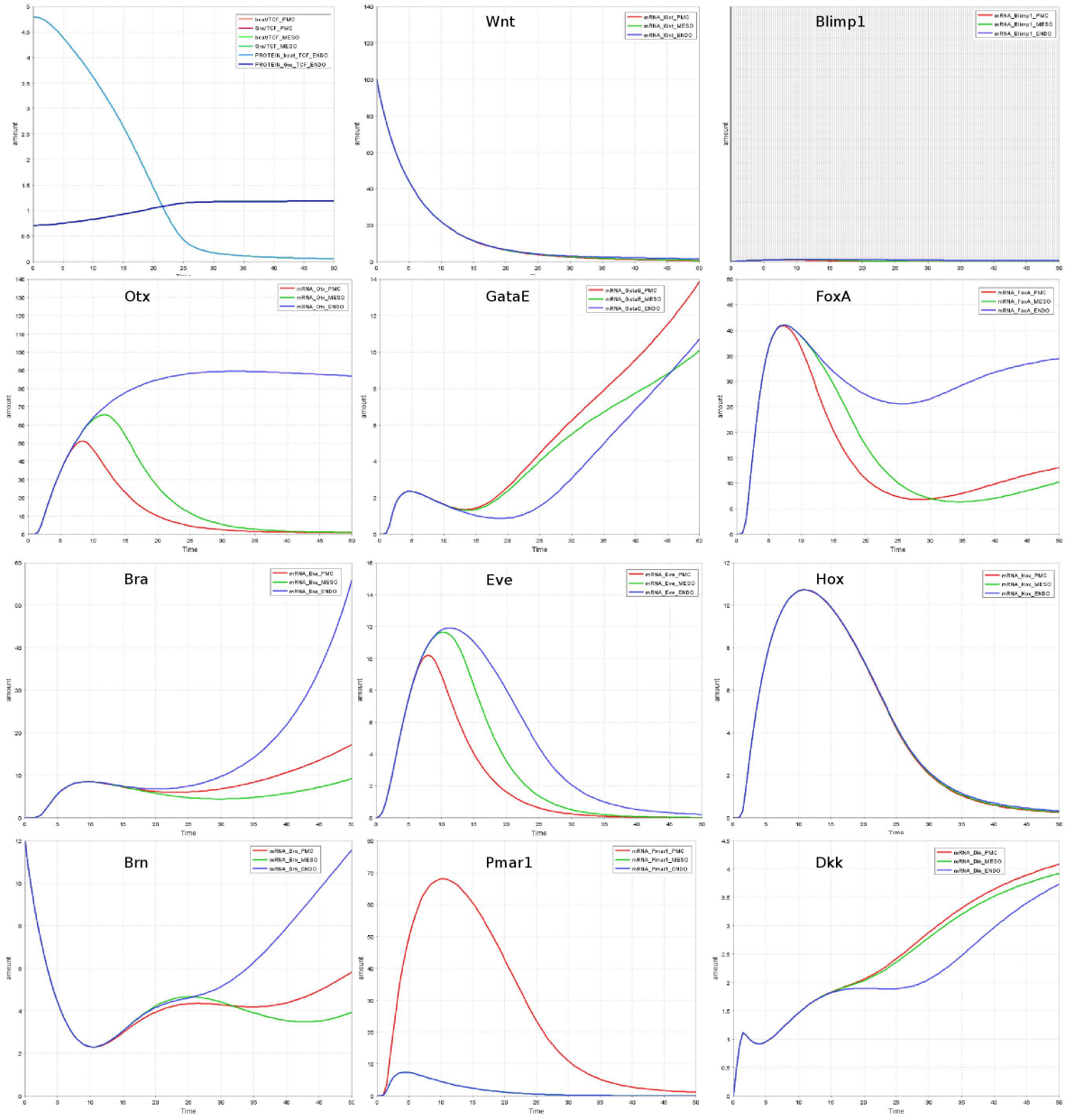

Figure 19: Simulations of the core model under *Blimp1* KO conditions. The x-axis shows hpf, the y-axis shows absolute transcript numbers per cell. Note that these plots have the same scales on the y-axis as in Fig.17 and analogous overlaps occur.

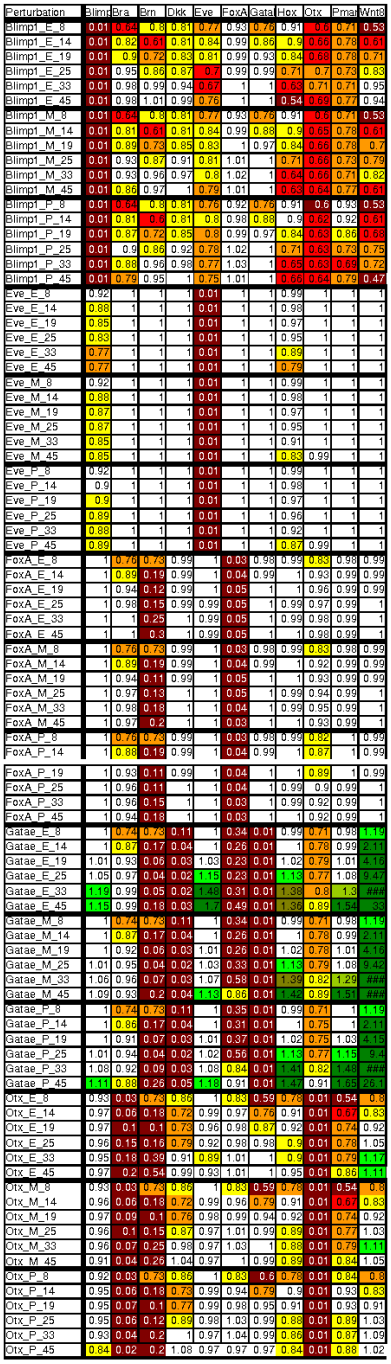

Perturbation	Blimp	Bra	Brn	Dkk	Eve	FoxA	Gata	Hox	Otx	Pmar	Wnt8
Blimp1_E_8	0.01	0.64	0.8	0.81	0.77	0.93	0.76	0.91	0.6	0.71	0.53
Blimp1_E_14	0.01	0.82	0.61	0.81	0.84	0.99	0.86	0.9	0.65	0.78	0.61
Blimp1_E_19	0.01	0.9	0.72	0.85	0.81	0.99	0.93	0.84	0.68	0.78	0.71
Blimp1_E_25	0.01	0.95	0.86	0.87	0.7	0.99	0.99	0.71	0.7	0.73	0.83
Blimp1_E_33	0.01	0.98	0.99	0.94	0.67	1	1	0.63	0.71	0.71	0.95
Blimp1_E_45	0.01	0.98	1.01	0.99	0.76	1	1	0.54	0.69	0.77	0.94
Blimp1_M_8	0.01	0.64	0.8	0.81	0.77	0.93	0.76	0.91	0.6	0.71	0.53
Blimp1_M_14	0.01	0.81	0.61	0.81	0.84	0.99	0.86	0.9	0.65	0.78	0.61
Blimp1_M_19	0.01	0.89	0.73	0.85	0.83	1	0.97	0.84	0.66	0.78	0.7
Blimp1_M_25	0.01	0.93	0.87	0.91	0.81	1.01	1	0.71	0.66	0.73	0.79
Blimp1_M_33	0.01	0.93	0.96	0.97	0.8	1.02	1	0.64	0.66	0.71	0.82
Blimp1_M_45	0.01	0.86	0.97	1	0.79	1.01	1	0.63	0.64	0.77	0.61
Blimp1_P_8	0.01	0.64	0.8	0.81	0.76	0.92	0.75	0.91	0.6	0.93	0.53
Blimp1_P_14	0.01	0.81	0.6	0.81	0.8	0.98	0.88	0.9	0.62	0.92	0.61
Blimp1_P_19	0.01	0.87	0.72	0.85	0.8	0.99	0.97	0.84	0.63	0.86	0.68
Blimp1_P_25	0.01	0.9	0.86	0.92	0.78	1.02	1	0.71	0.63	0.73	0.75
Blimp1_P_33	0.01	0.88	0.96	0.98	0.77	1.03	1	0.65	0.63	0.69	0.72
Blimp1_P_45	0.01	0.79	0.95	1	0.75	1.01	1	0.66	0.64	0.79	0.47
Eve_E_8	0.92	1	1	1	0.01	1	1	0.99	1	1	1
Eve_E_14	0.88	1	1	1	0.01	1	1	0.98	1	1	1
Eve_E_19	0.85	1	1	1	0.01	1	1	0.97	1	1	1
Eve_E_25	0.83	1	1	1	0.01	1	1	0.95	1	1	1
Eve_E_33	0.77	1	1	1	0.01	1	1	0.89	1	1	1
Eve_E_45	0.77	1	1	1	0.01	1	1	0.79	1	1	1
Eve_M_8	0.92	1	1	1	0.01	1	1	0.99	1	1	1
Eve_M_14	0.88	1	1	1	0.01	1	1	0.98	1	1	1
Eve_M_19	0.87	1	1	1	0.01	1	1	0.97	1	1	1
Eve_M_25	0.87	1	1	1	0.01	1	1	0.95	1	1	1
Eve_M_33	0.85	1	1	1	0.01	1	1	0.91	1	1	1
Eve_M_45	0.85	1	1	1	0.01	1	1	0.83	0.99	1	1
Eve_P_8	0.92	1	1	1	0.01	1	1	0.99	1	1	1
Eve_P_14	0.9	1	1	1	0.01	1	1	0.98	1	1	1
Eve_P_19	0.9	1	1	1	0.01	1	1	0.97	1	1	1
Eve_P_25	0.89	1	1	1	0.01	1	1	0.96	1	1	1
Eve_P_33	0.88	1	1	1	0.01	1	1	0.92	1	1	1
Eve_P_45	0.89	1	1	1	0.01	1	1	0.87	0.99	1	1
FoxA_E_8	1	0.76	0.73	0.99	1	0.03	0.98	0.99	0.83	0.98	0.99
FoxA_E_14	1	0.86	0.15	0.99	1	0.04	0.99	1	0.93	0.99	0.99
FoxA_E_19	1	0.94	0.12	0.99	1	0.05	1	1	0.96	0.99	0.99
FoxA_E_25	1	0.98	0.15	0.99	0.99	0.05	1	0.99	0.97	0.99	1
FoxA_E_33	1	1	0.25	1	0.99	0.05	1	0.99	0.98	0.99	1
FoxA_E_45	1	1	0.3	1	0.99	0.05	1	1	0.98	0.99	1
FoxA_M_8	1	0.76	0.73	0.99	1	0.03	0.98	0.99	0.83	0.98	0.99
FoxA_M_14	1	0.86	0.15	0.99	1	0.04	0.99	1	0.92	0.99	0.99
FoxA_M_19	1	0.94	0.11	0.99	1	0.05	1	1	0.93	0.99	0.99
FoxA_M_25	1	0.97	0.13	1	1	0.05	1	0.99	0.94	0.99	1
FoxA_M_33	1	0.99	0.18	1	1	0.04	1	0.99	0.95	0.99	1
FoxA_M_45	1	0.97	0.2	1	1	0.03	1	1	0.93	0.99	1
FoxA_P_8	1	0.76	0.73	0.99	1	0.03	0.98	0.99	0.82	1	0.99
FoxA_P_14	1	0.88	0.12	0.99	1	0.04	0.99	1	0.87	1	0.99
FoxA_P_19	1	0.93	0.11	0.99	1	0.04	1	1	0.89	1	0.99
FoxA_P_25	1	0.96	0.11	1	1	0.04	1	0.99	0.9	0.99	1
FoxA_P_33	1	0.96	0.15	1	1	0.03	1	0.99	0.92	0.99	1
FoxA_P_45	1	0.94	0.18	1	1	0.03	1	1	0.92	0.99	1
Gatae_E_8	1	0.74	0.73	0.11	1	0.34	0.01	0.99	0.71	0.98	1.19
Gatae_E_14	1	0.87	0.17	0.04	1	0.26	0.01	1	0.78	0.99	2.11
Gatae_E_19	1.01	0.93	0.06	0.03	1.03	0.23	0.01	1.02	0.79	1.01	4.16
Gatae_E_25	1.05	0.97	0.04	0.02	1.15	0.23	0.01	1.13	0.77	1.08	9.47
Gatae_E_33	1.19	0.99	0.05	0.02	1.48	0.31	0.01	1.38	0.8	1.3	###
Gatae_E_45	1.15	0.99	0.18	0.03	1.7	0.49	0.01	1.36	0.89	1.54	33
Gatae_M_8	1	0.74	0.73	0.11	1	0.34	0.01	0.99	0.71	0.98	1.19
Gatae_M_14	1	0.87	0.17	0.04	1	0.26	0.01	1	0.78	0.99	2.11
Gatae_M_19	1	0.92	0.06	0.03	1.01	0.26	0.01	1.02	0.78	1.01	4.16
Gatae_M_25	1.01	0.95	0.04	0.02	1.03	0.33	0.01	1.13	0.79	1.08	9.42
Gatae_M_33	1.06	0.96	0.07	0.03	1.07	0.58	0.01	1.39	0.82	1.29	###
Gatae_M_45	1.09	0.93	0.2	0.04	1.19	0.86	0.01	1.43	0.89	1.53	###
Gatae_P_8	1	0.74	0.73	0.11	1	0.35	0.01	0.99	0.71	1	1.19
Gatae_P_14	1	0.86	0.17	0.04	1	0.31	0.01	1	0.75	1	2.11
Gatae_P_19	1	0.91	0.07	0.03	1.01	0.37	0.01	1.02	0.75	1.03	4.15
Gatae_P_25	1.01	0.94	0.04	0.02	1.02	0.56	0.01	1.13	0.77	1.15	9.4
Gatae_P_33	1.08	0.92	0.09	0.03	1.08	0.84	0.01	1.41	0.82	1.48	###
Gatae_P_45	1.11	0.88	0.26	0.05	1.18	0.91	0.01	1.47	0.91	1.65	26.1
Otx_E_8	0.99	0.03	0.73	0.86	1	0.83	0.59	0.78	0.01	0.54	0.8
Otx_E_14	0.97	0.06	0.18	0.72	0.99	0.97	0.76	0.91	0.01	0.67	0.83
Otx_E_19	0.97	0.1	0.1	0.73	0.96	0.98	0.87	0.92	0.01	0.74	0.92
Otx_E_25	0.96	0.15	0.16	0.79	0.92	0.98	0.98	0.9	0.01	0.78	1.05
Otx_E_33	0.95	0.18	0.39	0.91	0.89	1.01	1	0.9	0.01	0.79	1.17
Otx_E_45	0.97	0.2	0.54	0.99	0.93	1.01	1	0.95	0.01	0.86	1.11
Otx_M_8	0.99	0.03	0.73	0.86	1	0.83	0.59	0.78	0.01	0.54	0.8
Otx_M_14	0.96	0.06	0.18	0.72	0.99	0.96	0.79	0.91	0.01	0.67	0.83
Otx_M_19	0.97	0.09	0.1	0.76	0.98	0.99	0.94	0.92	0.01	0.74	0.92
Otx_M_25	0.96	0.1	0.15	0.87	0.97	1.01	0.99	0.89	0.01	0.77	1.03
Otx_M_33	0.96	0.07	0.25	0.98	0.97	1.03	1	0.88	0.01	0.79	1.11
Otx_M_45	0.97	0.04	0.26	1.04	0.97	1	0.99	0.89	0.01	0.84	1.05
Otx_P_8	0.92	0.03	0.73	0.86	1	0.83	0.6	0.78	0.01	0.84	0.8
Otx_P_14	0.95	0.06	0.18	0.73	0.99	0.94	0.79	0.9	0.01	0.93	0.83
Otx_P_19	0.95	0.07	0.1	0.77	0.99	0.98	0.95	0.91	0.01	0.93	0.91
Otx_P_25	0.95	0.06	0.12	0.89	0.98	1.03	0.99	0.88	0.01	0.89	1.03
Otx_P_33	0.93	0.04	0.2	1	0.97	1.04	0.99	0.86	0.01	0.87	1.09
Otx_P_45	0.84	0.02	0.2	1.08	0.97	0.97	0.97	0.84	0.01	0.88	1.02

Figure 20: Effects of selected knock-outs in the core model using estimated parameters at selected timepoints. Rows indicate the knock-out and the celltype and timepoint. Columns show the selected genes. Each cell contains the ratio of transcript numbers for the indicated gene under the indicated knock-out by the number of transcripts without knock-out. Color codings indicate the size of the ratio r: downregulation: yellow ($0.8 < r \leq 0.9$), orange ($0.7 < r \leq 0.8$), red ($0.6 < r \leq 0.7$), dark red ($0.6 \geq r$), upregulation: light green ($1.1 < r \leq 1.2$), lime ($1.2 < r \leq 1.3$), tan ($1.3 < r \leq 1.4$), dark green ($1.4 <\leq r$)

KO'd GEN	effected	12 - 16	17 - 21	23 - 28	30 - 36	41 - 48
Blimp1	Eve	down	down	NA	NA	NA
	Otx	down	down	NA	NA	NA
	Wnt	NS	down	NS	NA	NA
Eve	GataE	NA	NA	down	NA	NA
	Hox	NS	down	down	NA	NA
	Blimp1	NS	NA	down	NA	NA
FoxA	Bra	NA	NS	NS	up	NS
	GataE	NA	NS	NS	NA	down
GataE	Bra	NA	down	down	down	NA
	FoxA	NA	down	down	NA	NA
	Wnt8	NA	down	NS	NA	NA
	Otx	NA	down	down	NA	NA
Otx	Bm	NA	NA	NA	NS	down

Figure 21: Portion of the perturbation data from [3] applicable to the core model

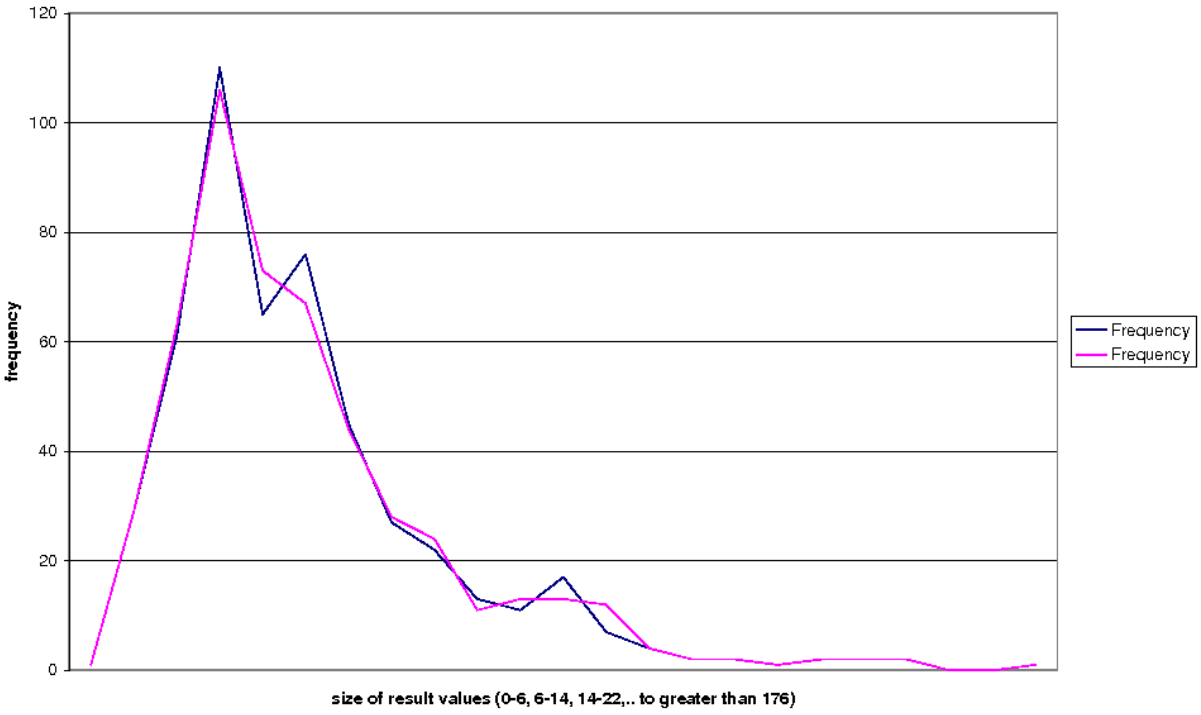

Figure 22: Distribution of simulation results for *Bra* at timepoint 8 under *Blimp1* knock-out and control conditions for all parameter sets.

M_p. Computation of $T2$ detected, as expected, more effects than $T1$. Using restrictive settings ($T1$), the algorithm detects significantly fewer results than under loose settings, indicating a more direct and palpable influence of the knocked out gene on the target or a stronger robustness to parameter changes for an interaction that is detected under the restrictive settings.

For the Wilcoxon signed rank test and the Kolmogorov-Smirnov test, a confidence interval of 95% was chosen. The findings of these tests differ from the findings of the counting algorithm. The Kolmogorov-Smirnov test detects even small differences very reliable. The Wilcoxon signed rank test on the other hand is over-sensitive for this application: For nearly all tested result pairs, the null-hypothesis that the pairs originate from the same distribution, was rejected.

The exact findings are included in the supplemental information, along with scatterplots for each pair of knock-out and effected gene. An example is depicted in Fig.23.

The strongest differences from Fig.23 are illustrated as scatterplots of the respective values in Fig.24.

To analyze the results of the different comparison methods, I characterized each species' concentrations at each time point measured in respect to how many of the comparison methods detected deviations between control and knock out simulation results. This characterization allows for easy assessment of the overall strength of the deviations: great changes are generally observable through the means regardless of their robustness. Robust changes are detected by the counting algorithm (small changes are only detectable under the loose threshold settings while strong changes should be detected under both loose and restrictive threshsold settings). Very small changes are only observable using the Kolmogorov-Smirnov test.

The results of this characterization, as depicted in Fig.25, show the following:

Blimp1-KO has a significantly detected downregulating effect on *Wnt8*, *Hox* and *Eve*, especially in PMC cells.

The knock-out of *Eve* has only slightly detected downregulating effects on *Blimp1* and *Hox*.

The effect of *FoxA* knock-out are also only slightly detectable as a reduction of *Brn* and *Otx* transcripts.

The effects of *GataE* knock-out are stronger: *Eve* transcription is only slightly dampened, *Brn* transcription is moderately reduced. Strongly detectable decline of transcript numbers applies to *Dkk* and *Otx*. An well detectable increase in transcript numbers is visible in the column depicting *Wnt8*.

The effects of *Otx* knock-out differ greatly between cell types: Endodermal expression is usually only effected up to 19 hpf, mesodermal expression is detectably effected up to 45 hpf and PMC expression is effected to the greatest extend throughout all timepoints. The only exception to this observation is the increase in transcript numbers of *FoxA*, which is strongest detected in endoderm and weakest in PMC. The only other gene upregulated by *Otx* knock-out is *GataE*. *Brn* is slightly downregulated at 8 hpf and then upregulated at 19 hpf (also 14 hpf in mesodermal cells). All other genes except for *Eve* are downregulated by *Otx* knock-out.

As with the estimated parameters, all effects occurring in one cell type also occur in the others, though the strength and duration of the effects varies between cell types.

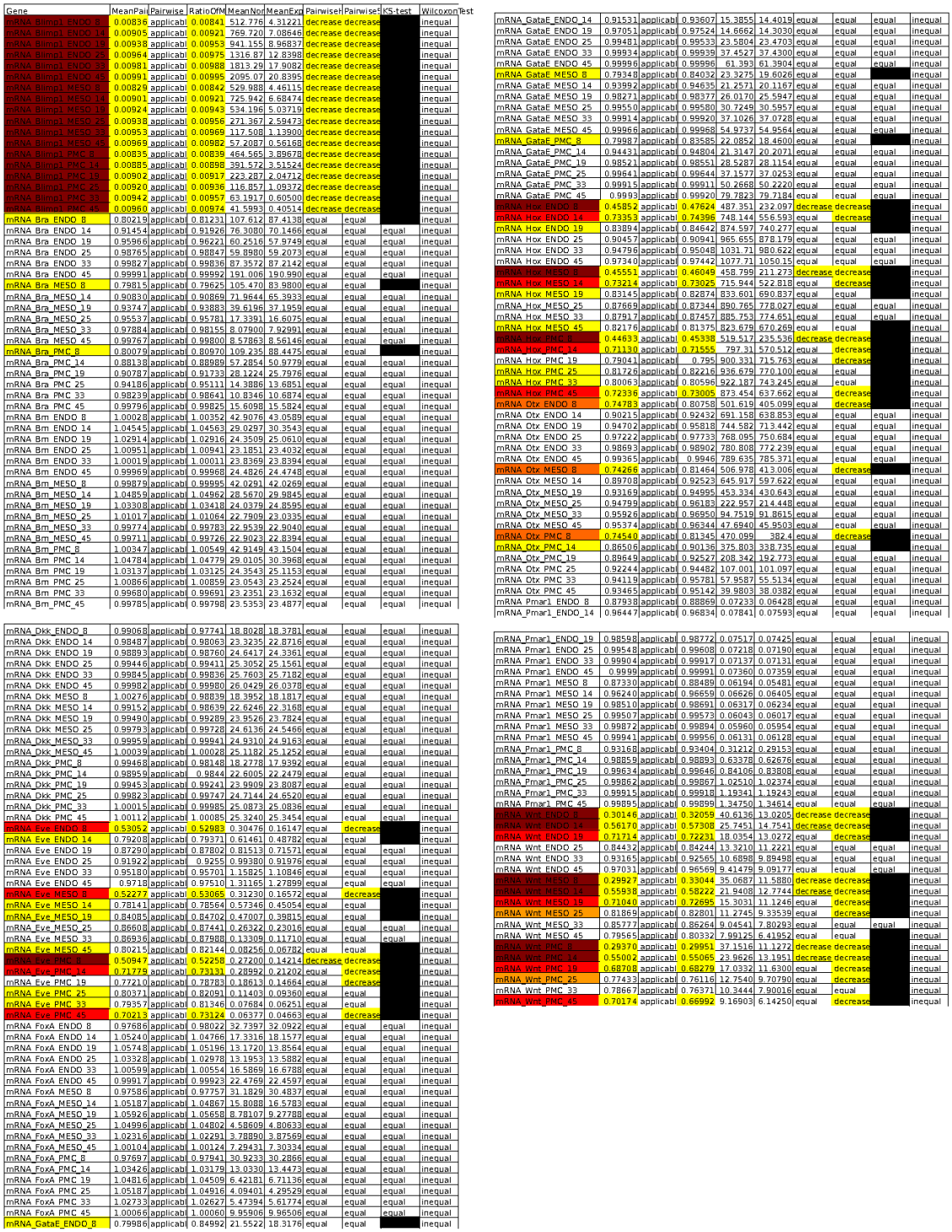

Figure 23: Analysis of the results of 500 simulations of the core model under both control and Blimp1 KO scenarios. The colors indicate decrease (yellow to dark red) or increase (light to dark green) of transcript numbers in *Blimp1* knock-out simulations compared to unperturbed simulations. Cells of the K-S column that are black indicate a difference detected in the Kolmogorov-Smirnov test. Notice that the Wilcoxon signed rank test detects differences everywhere using a 95% confidence interval.

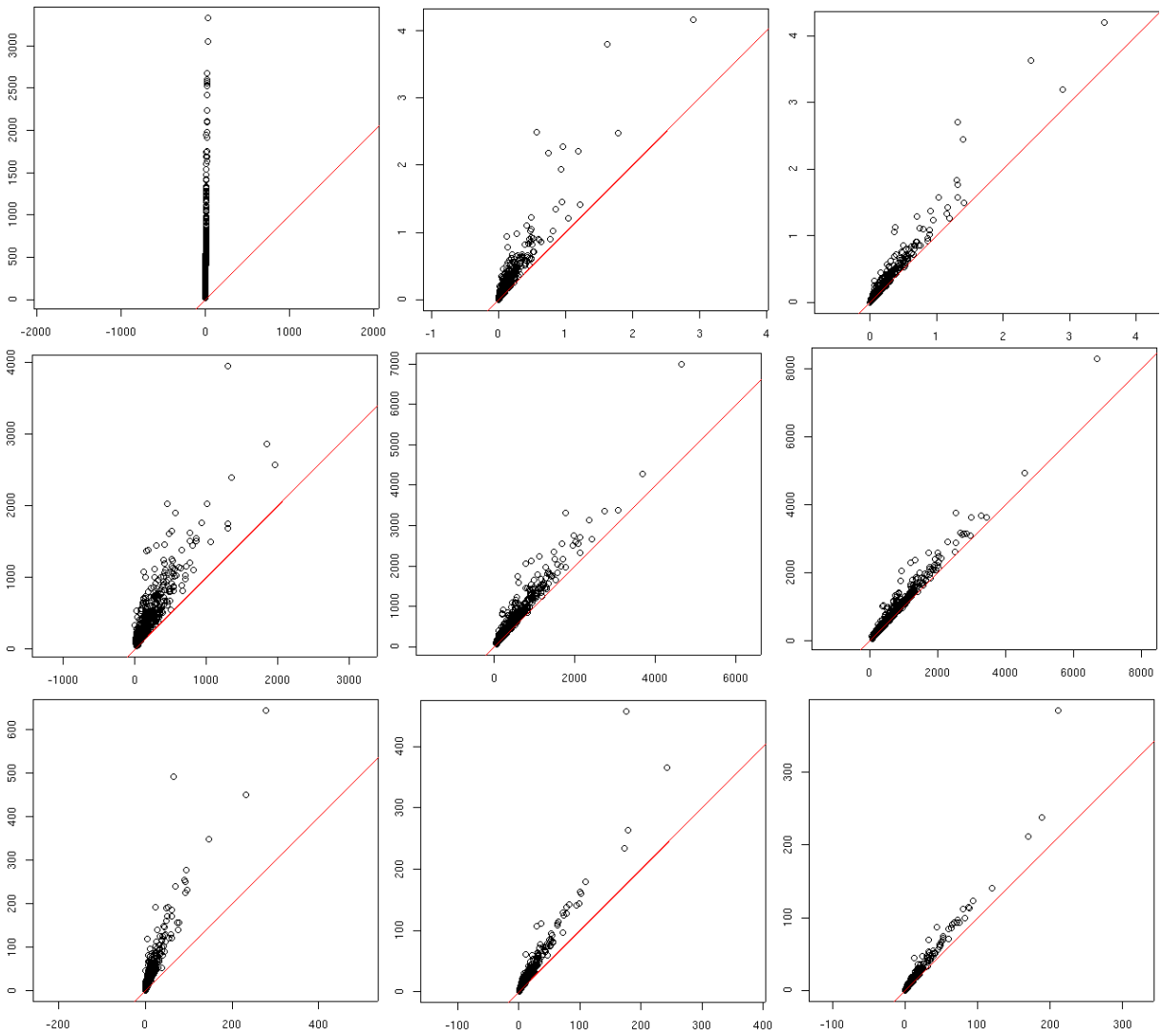

Figure 24: Scatterplots for selected pairs of control/Blimp1-KO simulation results. On the x-axis are the result values under knock-out conditions, on the y-axis are the result values under unperturbed conditions. Units are absolute transcript numbers per cell. Depicted from left to right, top to bottom are: Blimp1(endoderm) at timepoint 8, Eve(PMC) at timepoint 8 and 14, Hox (mesoderm) at timepoints 8,14,19, Wnt (endoderm) at timepoints 8,14,19.

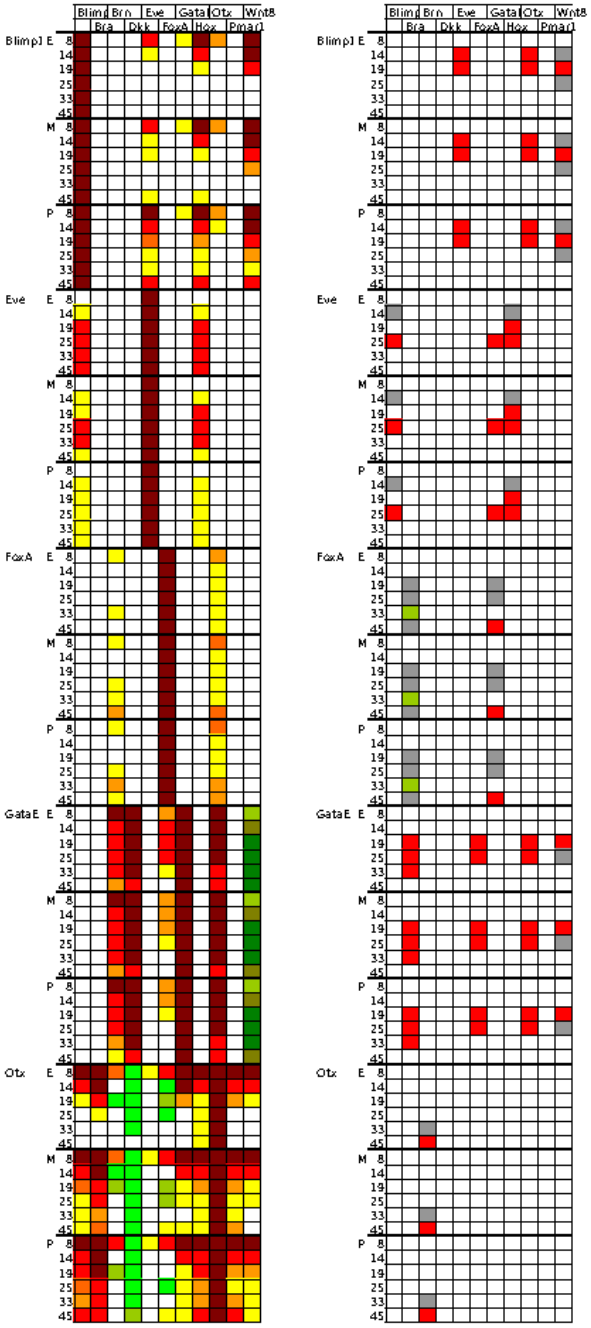

Figure 25: Overview of the characterized detected changes in the Core model using sampled parameters (left table) and the analogous experimental results (right table). Rows depict the knocked out genes and the spatiotemporal definition of the changes (E: Endoderm, M: Mesoderm, P: PMC cells). Columns indicate the effected genes. Color codings are as follows: yellow to dark red indicate decrease in transcriptional activity in growing detection intensity, light to dark green indicate increase in transcriptional activity. For the simulation data, white cells indicate no detectable effect of the perturbation. For the experimental results, grey cells indicate no significant detected changes and white cells represent effects for which no experimental data is available.

6.2 Endomesoderm model

The endomesoderm model contains too many unknown parameters to estimate parameters. Furthermore, experimental data to fit parameters is only available for a small fraction of the components. Therefore, no parameter estimation was performed on the Endomesoderm Network.

Instead, it was only simulated using sampled parameters. 500 parameters were sampled from a lognorm distribution with $\mu = 1.5$ and $\sigma^2 = 0.5$. The model was simulated using these 500 parameter sets for various conditions: unperturbed, *Alx1*-KO, *Blimp1*-KO, *Bra*-KO, *Brn*-KO, *Dri*-KO, *Ets1*-KO, *Eve*-KO, *FoxA*-KO, *FoxB*-KO, *GataC*-KO, *GataE*-KO, *Gcm*-KO, *Gsc*-KO, *Hnf6*-KO, *Hox*-KO, *Krl*-KO, *Otx*-KO, *Pmar1*-KO, *snail*-KO, *SoxB1*-KO and *Tbr*-KO. All of the named perturbations have counterparts in experimental data.

In simulations of the model and calculation of the artificial inputs, the time scale was multiplied by 10. Only endodermal conditions were considered. Because no realistic expression time curves are expected and the perturbations are assumed to have a similar effect in all tissues, this simplification is applicable.

Of the 500 simulations computed for each condition, only about 200 to 300 were successful. The failing of the simulations is mostly due to numerical reasons.

Since realistic expression time curves are not expected to be generated by the sampled parameters, the expression time cureves computed are not shown or discussed.

Thus, the results were only analyzed in respect to the perturbation experiments as with the core model. For the endomesoderm model, the means of both the paired values and the overall concentration means exhibit CVs (coeffiecients of variance) often exceeding 1 by multiple orders of magnitude. Since this indicates variances far greater than the mean, these mean values are excluded from the analysis. On the other hand, the Wilcoxon signed rank test produced more significant results than before. Since neither the Wilcoxon signed rank test, the Kolmogorov-Smirnov test or the counting algorithms showed sufficient to unambiguously detect effects of a perturbation, the scatterplots were included in the analysis.

Most of the 5922 produced scatterplots exhibit clear tendencies towards downregulation, upregulation or no regulation. Some have numerous outliers, indicating either effects very vulnerable to parameter changes or numerical issues hinted to above. Fig. 26 shows examples for both cases.

The scatterplots of certain KOs (*Otx* and *SoxB1*) exhibit more outliers than others. This is probably due to numerical difficulties arising in the simulation these KOs.

The results of the characterization of the effects from scatterplots are appended to tables showing the result of the statistical methods. To allow for comparison to experimental data, the experimentally detected effects were also included. An example is depicted in Fig.27

The cells of the tables are colored to allow for quick characterization of the detected effects. Red indicates downregulation by the perturbation for the counting algorithm, scatterplots and experimental data, green a respective upregulation and blue indicates effects detected by the K-S or Wilcoxon test.

As mentioned earlier, not all simulation runs finished successfully. When comparing the results of the experimental and control experiments, only those parameter sets are

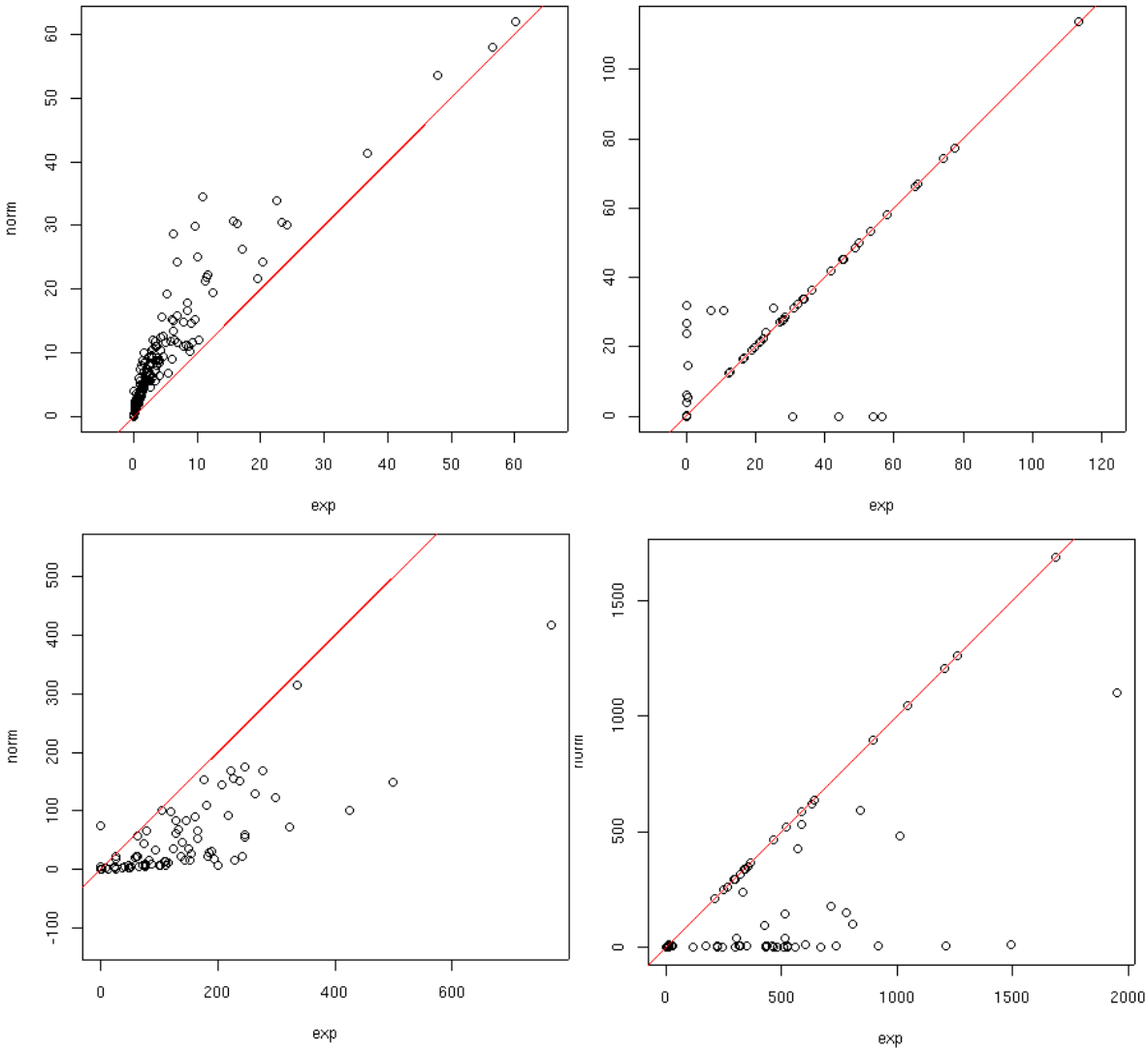

Figure 26: Scatterplots derived from the simulation results of the endomesoderm model. Shown are the concentrations under control conditions on the y-axis, concentrations under KO conditions on the x-axis. All graphs depict the measurementsat 25 hpf. Top left: effect of *FoxA*-KO on *Alx1*; bottom left: effect of *FoxA*-KO on *Dpt*. Both plots show obvious tendencies of the effect. Top right: effect of *Otx*-KO on *Brn*; bottom right: effect of *SoxB1*-KO on *FoxA*. These plots contain a great number of outliers that permit a unambiguous qualification of the depicted results.

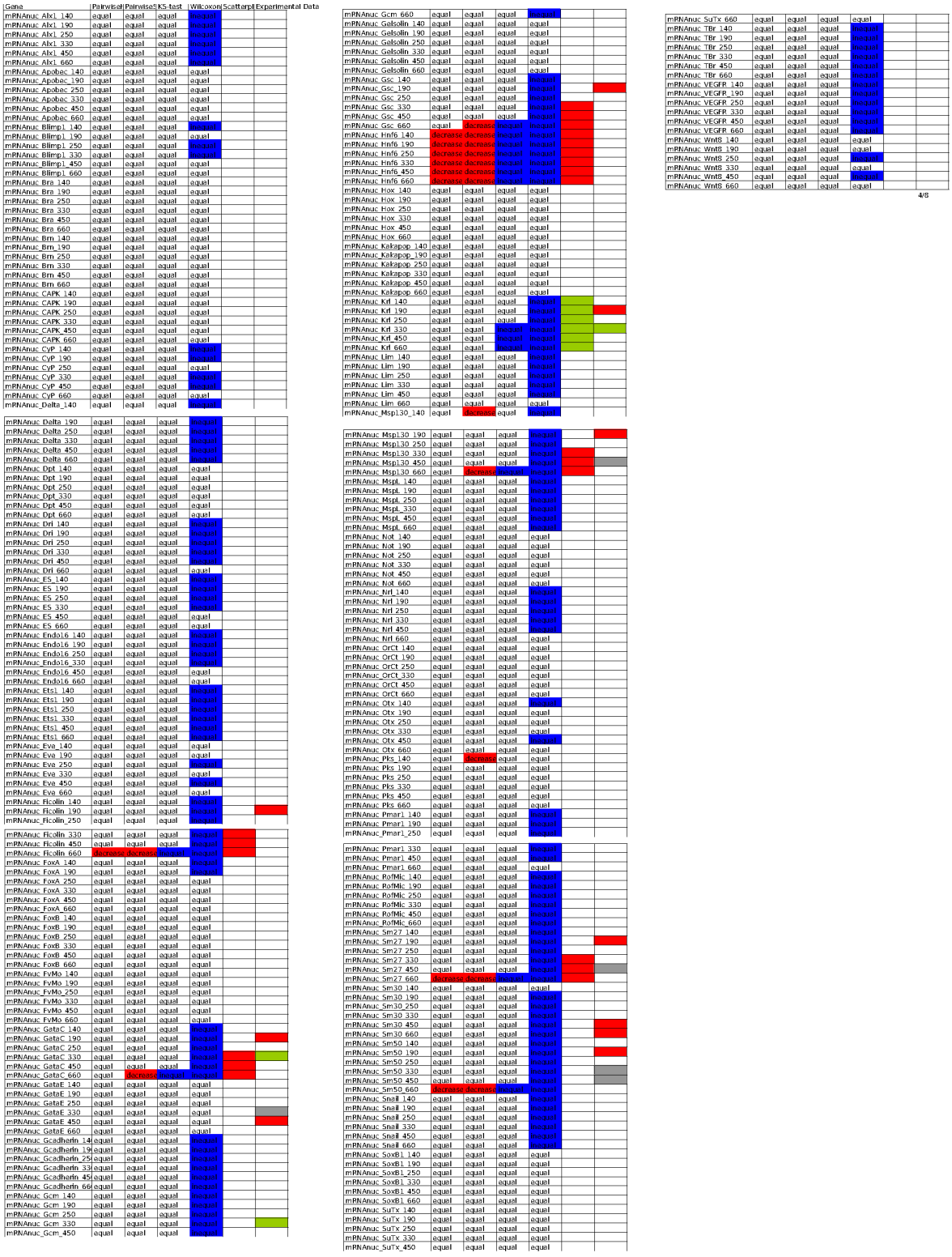

Figure 27: Example results for *in-silico* perturbation experiments on the Endomesoderm Network using sampled parameters. The example shown is *Hnf6*-KO. Color Codings are as explained in the text.

considered that have finished simulation runs under both perturbed and unperturbed conditions. Thus, the compared results differ in each case: *Alx1*-KO 187, *Blimp1*-KO 207, *Bra*-KO 274, *Brn*-KO 288, *Dri*-KO 203, *Ets1*-KO 199, *Eve*-KO 205, *FoxA*-KO 240, *FoxB*-KO 281, *GataC*-KO 197, *GataE*-KO 276, *Gcm*-KO 227, *Gsc*-KO 291, *Hnf6*-KO 194, *Hox*-KO 249, *Krl*-KO 293, *Otx*-KO 202, *Pmar1*-KO 203, *snail*-KO 271, *SoxB1*-KO 147 and *Tbr*-KO 188.

The sample size on which the the statistical tests are performed thus varies significantly in between experimental conditions and is generally about one half of the sample size used in the core model.

7 Discussion

7.1 Reproduction of Temproal Expression Data in the Core Model

The core model satisfactorily reproduces most temporal expression profiles and produces significantly different temporal expression profiles for the different cell types as described in section 6.1.1. For some genes, the temporal expression profile was not reproduced. These mismatches between experimental data and simulation results need refinement, which is - in the best case - based on the integration of new experimental data.

The most striking discrepancies between experimental data and simulation results apply to expression of *GataE* and *Hox*, for which spatial confinement of expression could not be reproduced. *Blimp1* and *Brn*, too, do not clearly exhibit spatial restriction. This lack of spatial confinement might be caused by missing repressors that mediate a default repression or by too little activator insufficiency (these two habits of developmental signaling pathways are described in section 2.1.3).

Experimentally determined expression of *FoxA* could also not be reproduced. The temporal expression pattern of *FoxA* exhibits an oscillatory behavior. Whether this behavior arises from changes in spatial restriction of *FoxA* expression, inhibition of *FoxA* expression by FoxA itself or other mechanisms (as interactions between *FoxA* and *Gcm*)is not determined yet. In the core model, I employed self-inhibition but using the estimated parameters, the oscillatory behavior could not be reproduced.

The simulated expression of *Dkk* also disagrees with experimental data. This is due to the design of the model but the aim was to include *Dkk* as a realistic suppressor of *Wnt8* activity - a key player in the model by this role - that is not included in the 'Endomesoderm Network'.

7.2 Reproduction of Perturbation Data in the Core Model

The need for more detailed experimental data is obvious when considering the experimental perturbation data. The simulation results show many effects which could not be verified or falsified because of missing data.

Where comparable experimental data is available, the core model was able to reproduce only about one half (8 of 15) of the experimentally determined effects correctly, indicating that the model demands refinement.

The effects of *Blimp1* MASO injection, namely a reduction in transcriptional activity of *Eve*, *Otx* and *Wnt8*, is correctly reproduced in the simulations of *Blimp1* knock-out.

The perturbation with *Eve* MASO leads to a reduction of *GataE*, *Hox* and *Blimp1* transcriptional activity in experiments. Of this experimental data, only the decline in *Blimp1* transcript numbers was accurately reproduced in simulation results using *Eve* knock-out conditions.

The experimental findings concerning *FoxA* MASO experiments are not reproduced by the simulation results at all.

GataE MASO injection leads to a decrease in *Bra*, *FoxA* and *Otx* transcript numbers reproduced in the according simulation results. The reduction in *Wnt8* transcriptional activity from experimental data is not reproduced in the simulation results. Instead, *Wnt8* transcriptional activity is increased in the simulation results.

The experimentally detected reduction of *Brn* transcription in *Otx* MASO experiments is accurately reproduced by the simulation results.

Thus, the Core model shows a high validity when considering only the temporal expression patterns. That it is not a sensible model that accurately captures the mechanisms underlying the endoderm and mesoderm specification in the early sea urchin embryo is shown by comparison of simulation results with experimental data of perturbation experiments. Some genes seem to be accurately modeled (i.e. *Otx*, *Blimp1*) while others show significant mismatches between simulation and experimental data (i.e. *FoxA* and *GataE*).

For some genes, the regulation chosen here seem to be correct (reproduction of temporal expression data, for example *Wnt8*). For other genes, their influence on target genes chosen here seems valid (reproduction of perturbation data, for example *Blimp1*). *Otx* seems to be realistically regulated but its influence on downstream target genes is flawed. *GataE* seems to neither be sensibly regulated nor does sensibly regulate. *GataE*, *FoxA* and the newly added *Dkk* are the genes for which the core model most urgently needs revision.

These necessary refinemets might concern simple rewiring of the involved interactions or the addition of new genes that give rise to more indirect interactions and enable more complex patterns of expression. Especially, since the experimental data also do not allow for a certain determination whether the effect of a perturbation is direct or indirect.

A general observation is that a number of specific activators has been found. But, as shown in section 2.1.3, spatial restriction of expression depends on inhibitory interactions. It is rather improbable that the endomesoderm specification network of the sea urchin contains so few inhibitory interactions compared to the number of activatory interactions.

7.3 Core Model and Sampled Parameters

The results of the simulated knock-outs using sampled parameters for the core model are described in section 6.1.4. I will first discuss to what extend they accurately reproduce the results of MASO experiments (depicted in Fig.21) and then describe how well they match the results of simulated knock-out experiments using the estimated parameters.

The experimental results exhibit an early decrease in transcriptional activity for *Eve* and *Otx* in case of *Blimp1* MASO injection. These results are accurately reproduced by the simulation results. The decline in *Wnt8* transcriptional activity under *Blimp1* MASO injection is reproduced, although the effect in the simulation results is strongest at 8 and

14 *hpf*, whereas this early decrease is not significantly detected in the experimental results.

Experimental data further indicates a fading in transcriptional activity for *GataE*, *Hox* and *Blimp1* when *Eve* MASO is injected. The reduction of *Hox* and *Blimp1* transcript numbers is reproduced in the knock-out simulation results while the drop of transcript numbers of *GataE* under knock-out conditions compared to normal is not reproduced at all.

When *FoxA* MASO is injected, experimental data shows significant increase in *Bra* transcription between 30 and 36 *hpf* and a decrease in *GataE* transcriptional activity between 41 and 48 *hpf*. Both experimental findings cannot be reproduced in the knock-out simulations.

The injection of *GataE* MASO leads to a decline in transcript numbers of *Bra*, *FoxA*, *Wnt8* and *Otx*. Although the reduction in *FoxA* and *Otx* transcriptional activity is reproduced in the knock-out simulation results, the reduction in *Bra* transcription rate is not reproduced and instead of a reduction of transcriptional activity for *Wnt8*, *Wnt8* is upregulated in the simulation results.

The experimental finding that, under *Otx* knock-out, *Brn* transcriptional activity declines can be accurately reproduced by the simulation results.

Altogether, five out of ten experimental results are reproduced in the simulations using sampled parameters.

In the following, I will compare the results of *in-silico* knock-out experiments using the sampled and the estimated parameters. Fig.28 illustrates this comparison.

The presented results indicate a high degree of matches between the two sets of results. Assuming that the estimated parameters are realistic, shades of green represent accordances between the two sets of results, shades of red in Fig.28 indicate false positives (effects in the realistic model not detected using the sampled parameters), Black indicates false negatives (effects detected using the sampled parameters that are not existent in the realistic model) and cells colored in blue represent changes detected in both sets of simulations but of opposite nature. For *Blimp1*, *Eve*, *FoxA* and *GataE*, most cells of the table show matches between the two sets of simulations with just a few false negatives and very few false positives. The part of the table depicting the comparison between *Otx* knock-out simulations show a significantly higher rate of false positives. This might be due to the high connectivity of *Otx* that leads to the establishment of perturbation effects downstream of the original perturbation.

Fig.29 shows a summary of the results. This summary shows that overall, about 73% of the single comparisons have similar indications while 16% reveal false negatives and the rate of false positives is about 8%. Whether these results only hold for relatively small models as the core model or whether they generally apply to the method of conducting simulations of knock-out experiments with sampled parameters remains to be determined. But the result indicate that the method can generate valid results.

The results of the Monte-Carlo knock-out simulations can further be used to characterize the robustness of the network. The scatterplots depicted in Fig.30 show an interaction robust to parameter changes: the scatterplots indicate a recovery of the concentration of *FoxA*-mRNA from the effects of the knock-out of *Otx*.

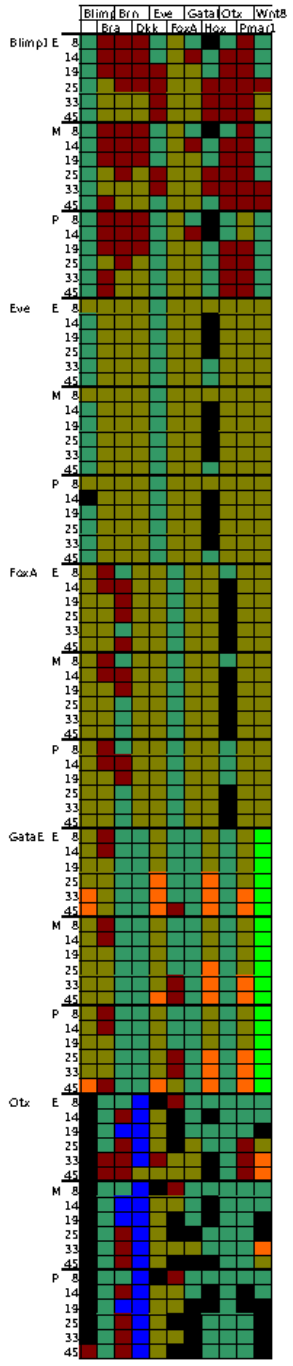

Figure 28: Comparison between simulated knock-out experiments using sampled and estimated parameters. Color codings indicate matches and mismatches between the two sets of simulations: shades of green indicate matches, shades of red indicate effects detected with the estimated parameters that are not detected using sampled parameters, blue indicates contrary effects in both sets of simulations, black indicates effects detected using sampled parameters that are not detected using the estimated parameters.

Category	frequency	percentage	cumulative %	
	18	0.018		
	430	0.43		
	286	0.29	0.738	
	27	0.027		
	127	0.13		
	21	0.021	0.178	0.916
	80	0.081	0.081	0.081
total	990			

Figure 29: Summary of the results presented in Fig.28. Color codings are accordingly: green indicates matches, red and orange false negatives, blue contradictory effects and black false positives. The second column shows the absolute numbers, the third column contains according percentages. columns four and five contain sums of percentages from top to bottom.

7.4 Reproduction of Perturbation Data and the Endomesoderm Model

The results of the *in-silico* experiments were compared to the experimental data based on the tables and scatterplots described in section 6.2.

As explained before, most of the scatterplots clearly indicate the effects (or absence of effects) of the KOs. In the cases of *SoxB1* and *Otx* though, numerous outliers were observed. These outliers generally form a parallel to the x- or y-axis, indicating expression either in control or experimental conditions and a complete shutdown of expression in the other condition(see Fig.26, bottom right plot). Often, both outliers on parallel to the y-axis and to the x-axis are observable (see Fig.26, top right panel). These outliers hint to a possible bistabilities of the system that are highly susceptible to parameter changes or changes in *SoxB1* and *Otx* expression. Further investigation of these phenomena might reveal intersting properties of the underlying topology.

To compare the computational and experimental data, matches between the two datasets need to be defined. I define a match between the two datasets if the effect of a perturbation on a gene's expression is detected at any timepoint in experimental data and a similar effect is detected at any timepoint in the simulated data. The two timepoints at which the effect is detected need not necessarily be the same. This time independence is necessary because first, the timescale in the simulation might be shifted, second because some effects are not clearly detected at the anticipated timepoint also a tendency towards this effect is palpable and third because experimental measurements are only available for a few timepoints. If a perturbation is shown to have a complex effect (first an increase and then a decrease in the effected gene's transcriptional activity, as the effect of *Hnf6*-KO on *Krl* expression for example), all different elements of the effect have to be reproduced in the correct temporal order in the computational data to produce a match.

For an effect to be detected as such in the simulation results, either the analysis of the scatterplots or according results of more than 2 of the statistical methods are required to indicate the effect.

The comparison of the detected effects is shown in Fig.31. As seen in the Fig.31, only 0.425 of the experimental data could be reproduced. This indicates that either the

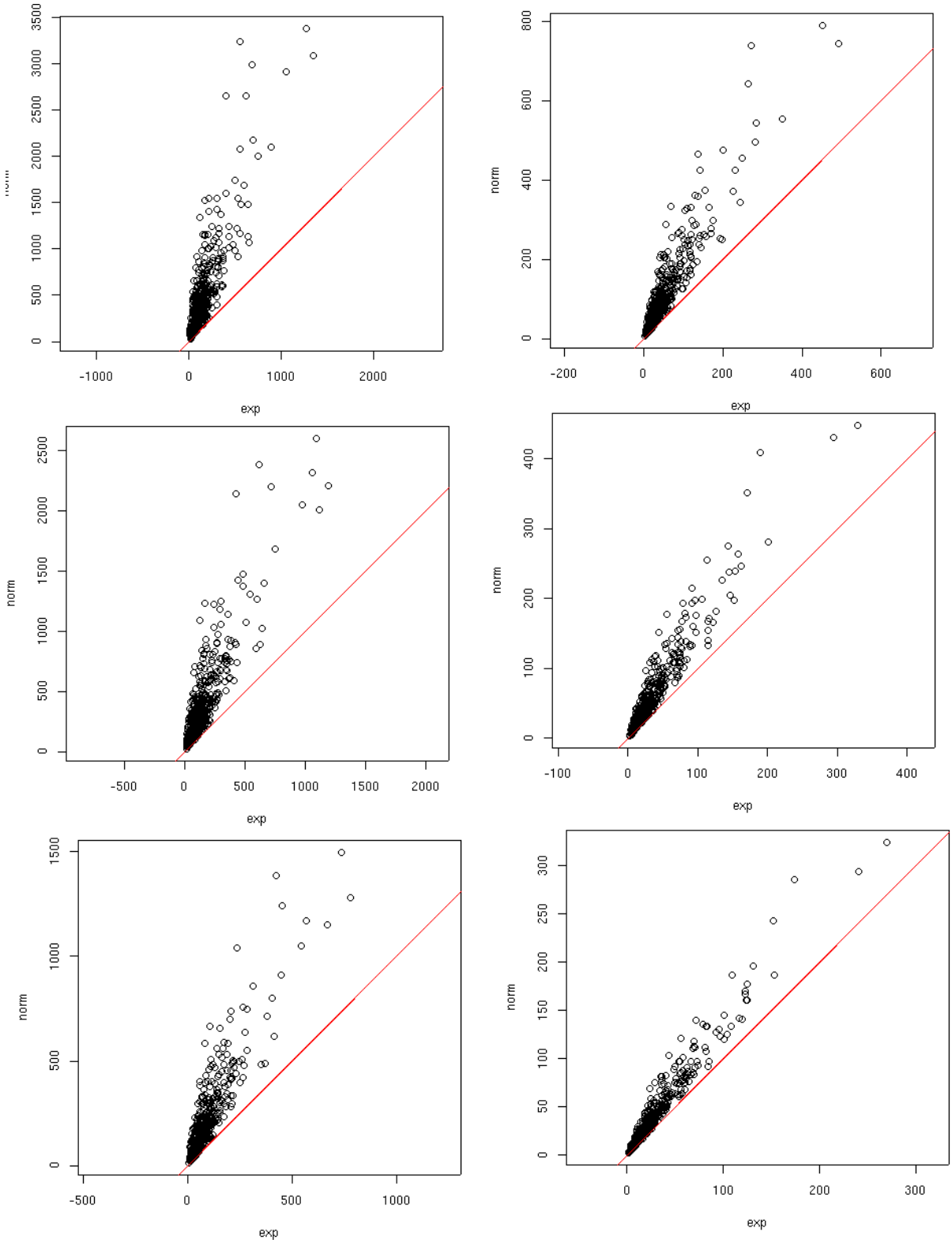

Figure 30: Scatterplots showing the robustness of *Otx* expression under *GataE*-KO in the core model. The plots show the results measured at 8 *hpf* (top left), 14 *hpf*, 19 *hpf* (bottom left), 25 *hpf* (top right), 33 *hpf* and 45 *hpf* (bottom right) Simulation results under control conditions are plotted on the y-axis, simulation results under *GataE*-KO conditions are plotted on the x-axis.

method used to generate the results is inapplicable or the model is flawed. I showed that the method is applicable to a smaller model and the results as depicted in Fig.26 are generally of comparable quality as the results for the core model (see Fig.24). I also mentioned that the 'Endomesoderm Network Model', which the 'endomesoderm model' is based on, contains some obvious flaws. Furthermore, the data that the network is based on is poorly documented.

Gene	Experiment	Simulation	Ratio
Alx1	9	6	0.667
Blimp1	3	3	1.000
Bra	12	1	0.083
Brn	3	0	0.000
Dri	9	6	0.667
Ets1	9	8	0.889
Eve	5	2	0.400
FoxA	8	2	0.250
FoxB	1	1	1.000
GataC	3	0	0.000
GataE	16	9	0.563
Gcm	4	4	1.000
Gsc	7	0	0.000
Hnf6	8	4	0.500
Hox	9	0	0.000
Krl	6	0	0.000
Otx	1	0	0.000
Pmar1	1	0	0.000
Snail	1	0	0.000
SoxB1	2	0	0.000
Tbr	5	3	0.600
Total	119	49	0.412

Figure 31: Comparison of experimental and simulated data for the endomesoderm model. Number of detected effects in experimental results and matching simulation results for the KO of each gene listed are shown. Totals are given at the bottom.

Reference [3] indicates that more experimental data exists, but this additional data is not available. This additional data is classified as 'Genes not effected or shown to be effected only indirectly'. Including this data into the comparison would greatly improve the result of the comparison because 'genes not effected' in experiments should also not be effected in simulation results when the model is valid and 'genes effected only indirectly' would also be detected in the simulation results if the model is valid. Additional data might thus help to clarify wether the model is valid or where it lacks correction in case it is invalid. How and why these genes were classified as irrelevant to the network topology is not explained and thus the whole quantification must be mistrusted.

Based on these facts, I conclude that the endomesoderm model, along with the underlying 'Endomesoderm Network Model' is erroneous. The topology of the model is unable to reproduce the experimental data and must be revised.

Additional information supporting this conclusion is produced by [1] (ongoing work): Experiments similar to those in [3] employing a slightly different set of genes show contradictory results, especially for those genes that produce the worst results here that are also investigated by [1] (*Gsc*, *Krl*). This indicates that the assumed inputs and outputs of *Gsc* and *Krl* are not realistic in the 'Endomesoderm Network Model'. The ongoing work might reveal evenmore misconceptions of the 'Endomesoderm Network Model' than the comparison of the simulation results to sparse experimental data could reveal.

When performing the revision of the network and models, special consideration should be payed to protein interactions, signaling pathways, ubiquitous repressors of transcriptional activity, the presumed key components of the network (as outlined in modeling the

core model) and computational methods to predict possible binding sites.

The determination of the correct TF binding sites is crucial because neither temporal expression curves nor perturbation experiments can unambiguously detect interactions between TFs and genes. Although computational prediction of binding sites is equally unreliable, it can serve as a basis for efficient experimental verification of TF-gene interactions.

7.5 'Core Genes' and Developmental Mechanisms

Since the set of 'core genes' used here and its function in development is expected to be conserved among most the deuterostomes [22], the implications gathered from the modeling and experimental analysis of the sea urchin might prove valuable for further research even in more complex species.

These 'core genes' are originally described as 'kernel' genes (*Blimp1*, *Otx*, *Bra*, *FoxA*, *GataE* and *Delta*) in [22]. The set of 'kernel genes' is based on observation that they are conserved among sea urchins and starfish, which diverged about half a billion years ago [22]. It is assumed that malfunction among any of these conserved genes has catastrophic effects on the developing embryo [22]. Since not all 'kernel genes' are modeled here and to avoid confusion, I termed the set of genes used in the small model 'core genes', because they are partly contained in the set of 'kernel genes' and are clearly the hubs (nodes having significant more edges than the other nodes) of the 'Endomesoderm Network'.

The simulation results show that malfunction of the kernel genes is not necessarily unrecoverable (see Fig.30).

I described a few developmental mechanisms in section 2.1.3. Of these established mechanisms, the most intricating seems to be the trinity of activator insufficiency, default repression and cooperative activation. Since many of the genes depicted in the 'Endomesoderm Network' 9 are activated by β-catenin/TCF, either the interaction between these genes and β-catenin/TCF as well as Groucho/TCF has to be experimentally validated or the interaction has to be changed to an indirect one since most of these genes are still expressed when Groucho/TCF is assumed to act as the default repressor. Furthermore, the models developed here should also be checked to whether they truly incorporate these mechanisms. Nevertheless, spatial confinement is not satisfactorily achieved in the core model. This is most certainly due to a lack of default repression.

Another important point to clarify when considering these developmental habits and the canonical Wnt pathway is the experimental data on TCF, β-catenin and Groucho. Since no data is available, one can either assume that TCF and Groucho concentrations are stable throughout development (thus leading to default inhibition from the time that nuclear β-catenin is depleted on) or that their concentrations also decrease from some point in development on (thus relieving the default inhibition mediated by Groucho/TCF).

7.6 Data

As mentioned numerous times before, the experimental data is very sparse. Although it seems to be sufficient to establish hypotheses about the molecular mechanisms controlling development of the sea urchin embryo, it seems to be quite insufficient to verify these

hypotheses. These hypotheses can also be verified by further experimental research, but computational (or computationally guided experimental) verification of the hypotheses is a cheaper and more efficient way.

Most temporal expression data is measured only at long intervals (sometimes only three measurements between fertilization and 60 *hpf*). This sparse data does not provide sufficient data to either estimate sensible parameters or verify a model from the reproduction of expression data.

No measurements of transcript numbers from early stages of development exist for most genes. This poses a huge problem to the simulation of ODE models, since no initial values are known.

As noted earlier, transcript numbers per embryo have to be recalculated to transcript numbers of cells expressing. A very basic approach has been proposed here (see section 3.2), which urgently needs refinement. The exact amount of cells constituting a certain territory and the exact spatial expression pattern need to be obtained. Then, the number of transcripts per cell needs further refinement in distinguishing between cells at the borders of territories of differential expression. Apart from recalculation of data obtained from whole embryos, isolated cells could be studied in which the concentrations of expected TFs that drive the expression of a certain target gene can be controlled externally.

Not only the expression data is too sparse. The perturbation data as given in [3] is just as sparse. Although it might be a utopistic view to test all perturbations on all possibly effected genes at numerous timepoints, the results of modeling can produce guidelines to which perturbations are necessary to provide experimental verification for a certain model. For more criticism on the available perturbation data, see 7.4.

Since the entire genome of *S.pur.* is available now, computational tools can be used to infer TF binding sites on assumed target genes. These inferred binding sites could then be verified using microarray screenings. Furthermore, the annotation of the $23,500$ genes can provide vital information and hint to parallels in other orgnanisms.

Another prominent part of the developmental program that is scarcely covered by experimental data is the part of protein interactions. Most of the parameters involved in protein interactions relevant to the development of sea urchins are unknown. Furthermore, it is not even experimentally validated that the canonical Wnt-pathway as depicted here is correctly applied to the sea urchin. Findings in *Xenopus*, for example, show that the Wnt-signaling network is very complex and uses multiple different subpathways for the transmission of different signals [80, 76].

Indications from ongoing experimental work of [1] show results contradictory to those given in [3]. If the new results prove to be correct, the whole data that the 'Endomesoderm Network Model' is based on must be scrutinized and the network likewise.

8 Conclusions and Outlook

The models presented in this work have been developed using the existing data. Both models fail to correctly reproduce all available data. This does not mean that the modeling was fruitless. The detection of errors in the established hypotheses concerning development in the sea urchin shows that modeling of these hypotheses should have been attempted before.

To refine the models and thus drive the research on developmental mechanisms, a closer collaboration between experimental and computational scientists is necessary. Based on the current experimental research, hypotheses about the developmental mechanisms are established. These can be formulated using mathematical models. Computational analysis of the models is used to falsify or verify the established hypotheses and thus guide experimental research. This combined approach should be complemented by further computational studies using the now available genome sequence of *S.pur.* and other resources.

These approaches can lead to an increasing amount of verified single-cell and simple multicellular models that each capture only rather atomic features of the whole developmental program.

Along with these insights, general characteristics of developmental GRNs will be determined, providing information urgently needed for the automated modeling of GRN from data. General characteristics can consist of topological features and their characterization (network motifs as described in section 2.2.1 , for example) or common dynamic features (habits of developmental GRNs as described in section 2.1.3, for example).

Using the metaphor of a disassembled car engine again, this increasing number of verified models corresponds to an increasing knowledge of the function and interplay of the various parts and subsystems of the engine. The amounting knowledge can - after exceeding a certain threshold - be employed to reconstruct the engine.

This reconstruction of the developmental program from single pathways and interactions will not be successful or satisfactory upon first attempt (as the models presented here), but exactly the made errors are the goal: To find incoherences between our understanding of the processes and their true behavior enables us to improve our understanding and refute false assumptions.

Supplemental Information

The SBML code of the Network and core models as well as detailed simulation results and documentation on parameter estimation are included on the CD. In case you have no CD, please try http://www.molgen.mpg.de/∼kuehn or http://www.mi.fu-berlin.de/∼ckuehn. Contents:

```
Thesis.pdf       electronic version of this document
Thesis.ps        likewise

models/          SBML-code of the ODE models and boolean
                 models in excel format
pet/             details of the parameter estimation
plots_Core/      scatterplots produced from the core model
                 and sampled parameters
plots_Endomes/   scatterplots produced from the Endomesoderm
                 Model and sampled parameters
models_KO/       models of the KO experiments using the
                 core model and estimated parameters
tables_Core/     tables used in the analysis of the core model
tables_Endomes/  tables used in the analysis of the
                 endomesoderm model
programs/        perl scripts and python programs used in this
                 thesis
```

References

[1] For information on the Group Evolution and Development at the Max-Planck-Institute for Molecular Genetics, Berlin, see http://www.molgen.mpg.de/ evolution-development/

[2] http://sbml.org/index.psp

[3] Website of the Davidson Lab with updated Networks and data: http://sugp.caltech.edu/endomes/. For an interactive version of the Endomesoderm Network Model, see http://sugp.caltech.edu/endomes/webStart/bioTapestry.jnlp

[4] Alon, U., Surette, M.G., Barkai, N., Leibler, S. 1997. Robustness in simple biochemical networks. Nature 387, 913

[5] Barabasi, A.-L., Albert, R. 1999. Emergence of Scaling in Random Networks. Science, 286, 509

[6] Barolo, S., Posakony J.W. 2002. Three habits of highly effective signaling pathways: principles of transcriptional control by developmental cell signaling. Genes and Development 16(10),1167-81

[7] Bolouri, H., Davidson E.H. 2002. Modeling DNA sequence-based *cis*-regulatory gene networks. Developmental Biology 246,2

[8] Bolouri, H., Davidson, E.H. 2002. Modeling transcriptional regulatory networks. BioEssays 24, 1118.

[9] Bolouri, H., Davidson E.H. 2003. Transcriptionalregulatory cascades in development: Initial rates, not steady states, determine network kinetics. Proceedings of the National Academy of Science 100(16), 9371

[10] Boveri, T. 1908. Zellenstudien VI: Die Entwicklung dispermer Seeigeleier. Ein Beitrag zur Befruchtungslehre und zur Theorie des Kerns. Jenaische Zeitschrift für Naturwissenschaften 43 (1)

[11] Buchler, N.E., Gerland, U., Hwa, T 2003. On schemes of combinatorial transcription logic. Proceedings of the National Academy of Science 100(9), 5136

[12] Ciliberto, A., Tyson, J.J. 2000. Mathematical Model for early development of the sea urchin embryo. Bulletin of Mathematical Biology 62, 37

[13] Croce, J., Lhomond G., Gache, C. 2001. Expression pattern of *Brachyury* in the embryo of the sea urchin *Paracentrotus lividus*. Development Genes Evolution 211, 617-619

[14] Croce, J., Duloquin, L., Lhomond, G., McClay, D.R., Gache, C. 2005. Frizzled5/8 is required in secondary mesenchyme cells to initiate archenteron invagination during sea urchin development. Development 133, 547.

[15] Croce, J.C., Wu, S.-Y., Byrum, C., Xu, R., Duloquin, L., Wikramanayake, A.H., Gache, C., McClay, D.R. 2006. A genome-wide survey of the evolutionary conserved Wnt pathways in the sea urchin *Strongylocentrotus purpuratus*. Developmental Biology 300(1),121-31

[16] Dan, K., Tanaka, S., Yamazaki, K., Kato, Y. 1980. Cell cycle study up to the time of hatching in the embryos of the sea urchin, hemicentrotus pulcherrimus. Development Growth and Differentiation 22, 589

[17] Daniels, D.L., Weis, W.I. 2005. β-catenin directly displaces Groucho/TLE repressors from TCF/Lef in Wnt-mediated transcription activation. Nature Structural and Molecular Biology 12(4), 364.

[18] von Dassow, G., Meir, E., Munro, E.M., Odell, G.M. 2000. The segment polarity network is a robust developmental module. Nature 406, 188

[19] Davidson, E.H. 1986. Gene Activity in Early Development, Third Edition. Academic Press

[20] Davidson E.H., al 2002. A Provisional regulatory gene network for specification of endomesoderm in the sea urchin embryo. Developmental Biology 246, 162-190

[21] Davidson, E.H. 2006. The sea urchin genome: where will it lead us? Science 314, 939

[22] Davidson, E.H., Erwin, D.H. 2006. Gene regulatory networks and the evolution of animal body plans. Science 311, 796

[23] Dean, J.L.E., Sully, G., Clark, A.R., Saklatvala, J. 2004. The involvement of AU-rich element-binding proteins in p38 mitogen-activated protein kinase pathway-mediated mRNA stabilization. Cellular Signalling, 16(10), 1113

[24] DeGroot, M.H. 1991. Chapter 9 in Probability an Statistics, 3rd ed. by Reading, MA. Addison-Weasly

[25] Ben-Tabou de-Leon, S., Davidson E.H. 2006. Deciphering the Underlying Mechanism of Specification and Differentiation: The Sea Urchin Gene Regulatory Network. Science Signal Transduction Knowledge Environment 361, 47

[26] Driesch, H. 1891. Entwicklungsmechanische Studien I. Der Wert der beiden ersten Furchungszellen in der echinodermententwicklung. Experimentelle Erzeugung von Teil- und Doppelbindungen. Zeitschrift für wissenschaftliche Zoologie 53, 160

[27] Ettensohn, C.E., Wessel, G.M., Wray, G. 1969. Development of Sea Urchins, Ascidians,and other Ivertebrate Deuterostomes: Experimental Approaches. Methods in Cell Biology 74

[28] Emily-Fenouil, F., Ghiglione, C., Lhomond, G., Lepage, T., Gache, C. 1998. GSK3β/shaggy mediates patterning along the animal-vegetal axis of the sea urchin embryo. Development 125, 2489.

[29] Finney, A., Hucka, M. 2003. Systems Biology Markup Language: Level 2 and Beyond Biochemical Society Transactions 31, 1472

[30] Fishman, G.S. 1995. Monte-Carlo: Concepts, Algorithms, and Applications. Springer Verlag, New York

[31] Funahashi, A., Tanimura, N., Morohashi, M., and Kitano, H. 2003. CellDesigner: a process diagram editor for gene-regulatory and biochemical networks, BIOSILICO, 1, 159

[32] Gibson, M.A., Mjolsness, E. 1999. Modeling the activity of singles genes. Computational Modeling of Genetic and Biochemical Networks. MIT Press WHEN

[33] Gilbert, S.F. 1994. Developmental Biology. Sunderland, MA: Sinauer Asscociates

[34] Gosset, W.S.('Student') 1908. The probable error of a mean. Biometrika 6, 1-25.

[35] Hill, A.V. 1910. The possible effects of the aggregation of the molecules of haemoglobin on its dissociation curves. Journal of Physiology 40, iv-vii

[36] Hertwig, O. 1876. Beiträge zur Kenntnis der Bildung, Befruchtung und Teilung des tierischen Eies. Gegenbaurs Morphologisches Jahrbuch 1, 374

[37] Howard-Ashby, M., Materna, S. C., Brown, C. T., Chen, L., Cameron, R.A., Davidson E. H. 2006. Identification and characterization of homeobox transcription factor genes in Strongylocentrotus purpuratus, and their expression in embryonic development. Developmental Biology (2006), doi:10.1016/j.ydbio.2006.08.039

[38] Hörstadius, S. 1939. The mechanics of sea urchin development, studied by operative methods. Biological Reviews 14, 132

[39] Huang, L., Li, X., El-Hodiri, H.M., Dayal, S., Wikramanayake, A.H., Klein, W.H. 1999. Involvement of Tcf/Lef in establishing cell types along the animal-vegetal axis of the sea urchins. Development Genes and Evolution 210, 73-81

[40] Hucka, M. et al. 203. The Systems Biology Markup Language (SBML): A Medium for Representation and Exchange of Biochemical Network Models. Bioinformatics 19(4), 524

[41] Hülsken, J., Behrens, J. 200. The Wnt signalling pathway. Journal of Cell Science 113, 3545

[42] Ji, X., Xu, Y. 2006. libSRES: a C library for stochastic ranking evolution strategy for parameter estimation. Bioinformatics 22, 124

[43] de Jong, H. 2002. Modeling and Simulation of Genetic Regulatory Systems: A Literature Review. Journal of Computational Biology, 9(1), 67-103

[44] Kashtan, N., Itzkowitz, S., Milo, R., Alon, U. 2002-2005, mfinder v1.2. http://www.weizmann.ac.il/mcb/UriAlon/

[45] Kell, D.B., Westerhoff, H.V. 1986. Metabolic control theory: its role in microbiology and biotechnology. FEMS Microbiol. Rev. 39, 305-320

[46] King, R.D., Whelan, K.E., Jones, F.M., Reiser, P.G.K., Bryant, C.H., Muggleton, S.H., Kell, D.B., Oliver, S.G. 2004. Functional genomic hypothesis generation and experimentation by a robot scientist. Nature 427, 247-252

[47] Klipp, E., Herwig, R., Kowald, A., Wierling, C., Lehrach, H. 2005. Systems Biology in Practice. Wiley-VCH, Weinheim.

[48] Krüger, R., Heinrich R. 2004. Model reduction and analysis of robustness for the Wnt/β-Catenin signal transduction pathway. Genome Informatics 15(1), 138

[49] Kühn, A. 2005. Klonierung und Charakterisierung von Dikkopf im Seeigel: Der Kopforganisator in einem kopflosen Tier. Diplomarbeit at the Freie Universität Berlin.

[50] Lee, E., Salic, A., Krüger, R., Heinrich, R., Kirschner M.W. 2003. The roles of APC and Axin derived from experimental and theoretical analysis of the Wnt pathway. PLos Biology 1(1), 116

[51] Lee, P.Y., Davidson, E.H. 2004. Expression of Spgatae, the Strongylocentrotus purpuratus ortholog of vertebrate GATA4/5/6 factors. Gene Expression Patterns 5,161165

[52] Li, X., Chuang, C.-K., Mao, C.-A., Angerer, L.M., Klein, W.H. 1997. Two Otx Proteins Generated from Multiple Transcripts of a Single Gene in Strongylocentrotus purpuratus. Developmental Biology 187, 253266.

[53] Livi, C.B. 2005. *Sp*blimp1/krox: A transcriptional regulator with a central role in endomesoderm specification in sea urchin embryos. http://resolver.caltech.edu/CaltechETD:etd-06052006-112833

[54] Livi, C.B., Davidson E.H. 2006. Expression and function of blimp1/krox, an alternatively transcribed regulatory gene of the sea urchin endomesoderm network. Developmental Biology 293, 513-525.

[55] Logan, C.Y., Miller, J.R., Ferkowicz, M.J., McClay, D.R. 1999. Nuclear β-catenin is required to specify vegetal cell fates in the sea urchin embryo. Development 126, 345

[56] Longabaugh, W.J.R., Davidson, E.H., Bolouri, H. 2005. Computational representation of developmental genetic regulatory networks. Developmental Biology 283, 1.

[57] Martins, G.G., Summers, R.G., Morill, J.B. 1998. Cells are added to the archenteron during and following secondary invagination in the sea urchin lytechinus variegatus. Developmental Biology 198, 330

[58] Masuda, M., Sato, H. 1984. Asynchronization of cell division is concurrently related with ciliogenesis in sea urchin blastulae. Development Growth and Differentiation 26, 281

[59] Miller, J.R., McClay, D.R. 1997. Changes in the pattern of adherens junction-associated beta-catenin accompany morphogenesis in the sea urchin embryo. Developmental Biology 192(2), 310-322

[60] Milo, R., Shen-Orr, S., Itzkowitz, S., Kashtan, N., Chklovski, D., Alon, U. 2002. Network Motifs: Simple Building Blocks of Complex Networks. Science, 298, 824

[61] Milo, R., Itzkowitz, S., Kashtan, N., Levitt, R., Shen-Orr, S., Ayzenshtat, I., Sheffer, M., Alon, U. 2004. Superfamilies of designed and evolved networks. Science 303, 1538-1542

[62] Minokawa, T., Rast, J.P., Arenas-Mena C., Franco, C.B., Davidson, E.H., 2004. Expression patterns of four different regulatory genes that function during sea urchin development. Gene Expression Patterns 4, 449

[63] Ochoa-Espinosa, A., Small, S. 2006. Developmental mechanisms and cis-regulatory codes. Current Opinion in Genetics & Development 16, 165

[64] Oliveri, P., Carrick, D.M., Davidson, E.H. 2002. A Regulatory Gene Network That Directs Micromere Specification in the Sea Urchin Embryo. Developmental Biology 246, 209228.

[65] Oliveri, P. , Walton, K.D., Davidson, E.H., McClay, D.R. 2006. Repression of mesodermal fate by foxa, a key endoderm regulator of the sea urchin embryo. Development 133, 4173-4181.

[66] Orphanides, G., Reinberg, D. 2002. A Unified Theory of Gene Expression. Cell 108(4), 439-451

[67] Petzold, L. 1983. Automatic selection methods for solving stiff and nonstiff systems of ordinary differential equations. Siam J Sci Stat Comput 4, 136-148

[68] Range, R.C., Venuti, J.M., McClay, D.R. 2004. LvGroucho and nuclear β-catenin functionally compete for TCF binding to influence activation of the endomesoderm gene regulatory network in the sea urchin embryo. Developmental Biology 279, 252.

[69] Ronen, M., Rosenberg, R., Shraiman, B.I., Alon, U. 2002. Assigning numbers to the arrows: Parameterizing a gene regulatory network by using accurate expression kinetics. Proceedings of the National Academy of Science 99(16), 10555

[70] Rosenfeld, N., Alon, U. 2003. Response delays and the structure of transcription networks. Journal of Molecular Biology 329,645

[71] Schilstra, M.J., Bolouri H. . Modelling the Regulation of Gene Expression in Genetic Regulatory networks. http://strc.herts.ac.uk/bio/maria/NetBuilder/Theory/NetBuilderModelling.htm

[72] Schilstra, M.J., Bolouri, H. 2002. The Logic of Gene Regulation. Proceedings of ICSB 2002: The Logic of Life, Karolinska Institutet, Stockholm, Sweden, Karolinska Institutet; pp 197-198

[73] Schilstra, M. 2003. Netbuilder. http://strc.herts.ac.uk/bio/maria/NetBuilder/

[74] Sea Urchin Genome Sequencing Consortium, 2006. The Genome of the sea urchin Strongylocentrotus Purpuratus. Science 314, 941

[75] Summers, R.G., Morill, J.B., Leith, J., Marko, M., Piston, D.W., Stonebraker, A.T. 1993. A stereometric analysis of karyokinesis, cytokinesis and cell arrangements during and following fourth cleavage period in the sea urchin, Lytechinus Variegatus. Development Growth and Differentiation 35, 41

[76] Tada, M., Smith, J.C. 2000. Xwnt11 is a target of Xenopus Brachyury: regulation of gastrulation movements via Dishevelled, but not through the canonical Wnt pathway. Development 127, 2227-2238.

[77] Tanaka, S., Dan, K. 1990. Study of the lineage and cell cycle of small micromeres in the embryos of the sea urchin, Hemicentrotus pulcherrimus. Development Growth and Differentiation 32, 145

[78] Vonica, A., Weng, W., Gumbiner, B.M., Venuti, J.M. 2000. TCF is the nuclear Effector of the β-catenin signal that patterns the sea urchin animal-ventral axis. Developmental Biology 217, 230.

[79] Waage, P., Guldberg, C.M. 1864. Forhandlinger: Videnskabs-Selskabet i Christiana 1864, 35

[80] Wallingford, J.B., Vogeli, K.M., Harland, R.M. 2001. Regulation of convergent extension in Xenopus by Wnt5a and Frizzled08 is independent of the canoncial Wnt pathway. International Journal of Developemtental Biology 45,225-227.

[81] Weitzel, H.E., Illies, M.R., Byrum, C.A., Xu, R., Wikramanayake, A.H., Ettensohn, C.A. 2003. Differential stability of β-catenin along the animal-ventral axis of the sea urchin embryo mediated by dishevelled. Development 131, 2947.

[82] Wikramanayake, A.H., Peterson, R., Chen, J., Huang, L., Bince, J.M., McClay,D.R., Klein, W.H. 2004. Nuclear β-Catenin-Dependent Wnt8 Signaling in Vegetal Cells of the Early Sea Urchin Embryo Regulates Gastrulation and Differentiation of Endoderm and Mesodermal Cell Lineages. Genesis 39, 194-205.

[83] Wierling, C. 2006. PyBioS - ein Modellierungs- und Simulationssystem für komplexe biologische Prozesse. In: Forschung und wissenschaftliches Rechnen. Beiträge zum Heinz-Billing Preis 2005. Gesellschaft für wissenschaftliche Datenverarbeitung Göttingen.

[84] Wilcoxon, F. 1945. Individual comparisons by rnking methods. Biometrics 1, 80-83.

[85] Yuh, C.-H., Dorman, E.R., Howard, M.L., Davidson E.H. 2004. An *cis*-regulatory module: a key node in the sea urchin endomesoderm gene regulatory network. Developmental Biology 269, 536-551

[86] Yuh, C.-H., Dorman, E.R., Davidson, E.H. 2005. Brn1/2/4, the predicted midgut regulator of the endo16 gene of the sea urchin embryo. Developmental Biology 281, 286-298.

[87] Zi, Z., Klipp, E. 2006. SBML-PET: a systems biology markup language based parameter estimation tool. Bioinformatics 2006, doi:10.1093/bioinformatics/btl443

Eidesstattliche Erklärung

Ich erkäre hiermit an Eides Statt, dass ich die vorliegende Arbeit selbstständig und ohne Benutzung anderer als der angegebene Hilfsmittel angefertigt habe; die aus fremden Quellen direkt oder indirekt überenommenen Gedanken sind als solche kenntlich gemacht.

Die Arbeit wurde bisher in gliecher oder ähnlicher Form keiner anderen Prüfungskomission vorgelegt und auch nicht veröffentlicht.

Berlin, den 20.12.2006